

Contents lists available at ScienceDirect

#### Journal of Controlled Release

journal homepage: www.elsevier.com/locate/jconrel





### PEGylated nanoparticles interact with macrophages independently of immune response factors and trigger a non-phagocytic, low-inflammatory response

Monireh Asoudeh <sup>a,1</sup>, Nicole Nguyen <sup>b,1</sup>, Mitch Raith <sup>a</sup>, Desiree S. Denman <sup>a</sup>, Uche C. Anozie <sup>a</sup>, Mahshid Mokhtarnejad <sup>a</sup>, Bamin Khomami <sup>a</sup>, Kaitlyn M. Skotty <sup>a</sup>, Sami Isaac <sup>a</sup>, Taylor Gebhart <sup>c</sup>, Lauren Vaigneur <sup>d</sup>, Aga Gelgie <sup>e</sup>, Oudessa Kerro Dego <sup>e</sup>, Trevor Freeman <sup>e</sup>, Jon Beever <sup>e</sup>, Paul Dalhaimer <sup>a,\*</sup>

- <sup>a</sup> Department of Chemical and Biomolecular Engineering, University of Tennessee, Knoxville, TN 37996, USA
- <sup>b</sup> School of Medical Laboratory Science, University of Tennessee Medical Center, Knoxville, TN 37996, USA
- Centre College, Danville, KY 40422, USA
- <sup>d</sup> Brigham Young University Idaho, Rexburg, ID 83460, USA
- <sup>e</sup> Animal Science, University of Tennessee, Knoxville, TN 37996, USA

#### ARTICLE INFO

#### Keywords: PEG Macrophage Inflammation Liposome Phagocytosis Lipoprotein Autophagy

#### ABSTRACT

Poly-ethylene-glycol (PEG)-based nanoparticles (NPs) - including cylindrical micelles (CNPs), spherical micelles (SNPs), and PEGylated liposomes (PLs) - are hypothesized to be cleared in vivo by opsonization followed by liver macrophage phagocytosis. This hypothesis has been used to explain the rapid and significant localization of NPs to the liver after administration into the mammalian vasculature. Here, we show that the opsonizationphagocytosis nexus is not the major factor driving PEG-NP - macrophage interactions. First, mouse and human blood proteins had insignificant affinity for PEG-NPs. Second, PEG-NPs bound macrophages in the absence of serum proteins. Third, lipoproteins blocked PEG-NP binding to macrophages. Because of these findings, we tested the postulate that PEG-NPs bind (apo)lipoprotein receptors. Indeed, PEG-NPs triggered an in vitro macrophage transcription program that was similar to that triggered by lipoproteins and different from that triggered by lipopolysaccharide (LPS) and group A Streptococcus. Unlike LPS and pathogens, PLs did not increase transcripts involved in phagocytosis or inflammation. High-density lipoprotein (HDL) and SNPs triggered remarkably similar mouse bone-marrow-derived macrophage transcription programs. Unlike opsonized pathogens, CNPs, SNPs, and PLs lowered macrophage autophagosome levels and either reduced or did not increase the secretion of key macrophage pro-inflammatory cytokines and chemokines. Thus, the sequential opsonization and phagocytosis process is likely a minor aspect of PEG-NP - macrophage interactions. Instead, PEG-NP interactions with (apo)lipoprotein and scavenger receptors appear to be a strong driving force for PEG-NP - macrophage binding, entry, and downstream effects. We hypothesize that the high presence of these receptors on liver macrophages and on liver sinusoidal endothelial cells is the reason PEG-NPs localize rapidly and strongly to the liver.

Abbreviations: BMDM, bone-marrow-derived macrophages; BSA, bovine serum albumin; CNP, cylindrical micelle nanoparticle; DLS, dynamic light scattering; DMEM, Dulbecco's Modified Eagle Medium; DSPE, 1,2-distearoyl-sn-glycero-3-phosphoethanolamine; FBS, Fetal bovine serum; FPKM, fragments per kilobase of transcript per million mapped reads; γG, γ-globulin; HDL, high-density lipoprotein; HPLM, human-plasma-like media; KEGG, Kyoto encyclopedia of genes and genomes; LDL, low-density lipoprotein; LIMP-2, lysosomal integral membrane protein-2; LNP, lipid nanoparticle; LPS, lipopolysaccharide; MARCO, macrophage receptor with collagenous structure; NIR, near infrared; NP, nanoparticle; NSG, NOD scid gamma immunodeficient mice; oxLDL, oxidized low-density lipoprotein; PAMPs, pathogen-associated molecular pattern molecules; PBD, polybutadiene; PC, phosphatidylcholine; PCA, principal component analysis; PEG, poly-ethylene-glycol; PEO, poly-ethylene-oxide; PL, PEGylated liposome; PRR, pattern recognition receptor; P-S, penicillin-streptavidin; ROS, reactive oxygen species; SNP, spherical micelle nanoparticle; SR-A, scavenger receptor A; TLR, toll-like receptor; TPM, transcripts per million; VLDL, very low density lipoprotein.

E-mail address: pdalhaim@utk.edu (P. Dalhaimer).

<sup>\*</sup> Corresponding author: Associate Professor of Chemical and Biomolecular Engineering, University of Tennessee, 426 Dougherty Engineering Building, 1512 Middle Drive, Knoxville, TN 37996, USA.

 $<sup>^{1}\,</sup>$  M.A. and N.N. contributed equally to this work.

#### 1. Introduction

Fluid nanoparticles (NPs), whose exteriors are comprised of ~5-to-100 mol% poly-ethylene-glycol (PEG) or poly-ethylene-oxide (PEO), that circulate in the mammalian vasculature, localize rapidly to the liver [1]. The most common hypothesis for this phenomenon is that immune response factors in the blood bind the PEG-based NPs (PEG-NPs). A subset of the bound proteins could be pre-existing immunoglobulins raised against non-PEG challenges or immunoglobulins raised specifically against PEG from previous exposures [2]. The immunoglobulins bound to PEG-NPs would then bind Fc receptors (FcR) on the surfaces of liver macrophages where the PEG-NP would be internalized by phagocytosis and degraded in a lysosome or an autolysosome [3]. The complement system could also play a key role in delivering PEG-NPs to liver macrophages. For this to happen, at least one of the following three scenarios would have to occur. The classical complement pathway would need to be triggered by an antibody against PEG-NPs to which C1q, C1r, and C1s would bind; PEG would need to be recognized as a sugar for the lectin complement pathway to be activated; or PEG would need to hydrolyze the main complement factor, C3, for the alternative pathway to be activated.

Yet, macrophages play multiple roles in mammalian physiology beyond foreign particle clearance. Liver macrophages are key regulators of metabolic equipoise. They take up lipoproteins through their lipoprotein and scavenger receptors [4]. Relevant to this study, the apolipoproteins ApoA-I, ApoB-100, ApoC-III, and ApoE form a significant fraction of the still sparse PEG-NP protein corona when the percent of NP components that are PEGylated is low (i.e., less than  $\sim$ 5 mol%) [5–8]. On the other hand, immunoglobulins and complement have relatively low presence in or on PEG-NP protein coronas in the same studies [5–8]. The above apolipoproteins are structural components of chylomicrons, high-density lipoprotein (HDL), low-density lipoprotein (LDL), and very low-density lipoprotein (VLDL). Thus, a second hypothesis was formed in which apolipoproteins bind and take PEG-NPs to (apo)lipoprotein receptors on macrophage surfaces. Indeed, soft lipid NPs (~2% PEG) carrying CRISPR-Cas9 reagents appeared to enter human hepatocytes in vivo through the LDL receptor (LDLR) via ApoE presence on the surface of the NP [7]. ApoE (and possibly other apolipoproteins) [9] appears to be a strong driver of NP - cell uptake when the NP has a high lipid content and a low PEG and/or sheddable PEG content [10,11].

A third hypothesis has emerged in which the PEG of the PEG-NP directly binds cell surface receptors. In this scenario, PEG could trigger a pathogen-associated molecular pattern molecule (PAMP) pattern recognition receptor (PRR) response, such as the binding of the strongly pro-inflammatory lipopolysaccharide (LPS) to toll-like receptor 4 (Tlr4) or to scavenger receptors such as MARCO [12]. It is also possible that the PEG-receptor pairing could be tolerated/benign [1]. X-ray scattering uncovered the presence of PEG deep in the cholesterol binding pocket of LIMP-2 [13]. LIMP-2 is a member of the CD36 superfamily of proteins along with scavenger receptor class B I (SR-BI) [13]. The CD36 family of proteins function as lipoprotein receptors and cholesterol and fatty acid transporters. The long-term presence of PEG in the interior of LIMP-2 during crystal formation suggests that PEG binds LIMP-2. Molecular dynamics simulations confirmed that PEG can penetrate the LIMP-2 cholesterol binding pocket and form multiple hydrogen bonds with the residues in the pocket [14]. Furthermore, free PEG and PEG-NP micelles bind reconstituted SR-BI with micromolar affinity [1]. PEG-NP micelles are internalized by cells expressing SR-BI [1]. The signal of 100% PEGylated NPs was significantly lowered in the livers of  $SCARB1^{-/-}$  mice (the gene that codes for SR-BI) over the livers of wild-type mice [1]. Co-injecting these PEG-NPs with hHDL, in a competition experiment, into wild-type mice also significantly lowered the NP signal in the livers of these animals [1]. SR-A (macrophage scavenger receptor A), the main receptor for oxidized LDL (oxLDL) is also an intriguing factor in PEG-NP uptake because its pharmacological blockage lowers PEG-NP micelle signal in macrophage incubations [1].

The same is true of MARCO, which appears to play a role in PEG-polystyrene biodistribution [12]. Thus, it appears that PEG itself and PEG-NPs can directly bind lipoprotein receptors and scavenger receptors.

We aimed to test the above three PEG-NP - macrophage interaction models: 1) PEG-NPs are opsonized and phagocytosed as foreign objects, 2) apolipoproteins jump from lipoproteins to PEG-NPs after which the apolipoprotein-PEG-NP complex binds (apo)lipoprotein receptors through the pre-existing apolipoprotein-receptor affinity, and 3) PEG on the NP directly binds macrophage surface receptors. We chose PEG-based cylindrical micelles (CNPs) as a model for long-circulating NPs, PEG-based spherical micelles (SNPs) as a model for classical spherical micelles, and the PEGylated lipid bilayer vesicle DOXIL (PL), which is used in the clinic (PL), as a model for a PEGylated liposome. The PLs used here do not contain doxorubicin. We chose these varying NPs to broaden the impact of our findings across 1) percent PEGylated (100% for CNPs and SNPs versus 5% for PLs), 2) geometry (cylindrical CNPs versus spherical SNPs), and 3) 100% synthetic chemistries for CNPs and SNPs versus lipid-based chemistries for PLs.

#### 2. Materials and methods

#### 2.1. Nanoparticles, lipoproteins, JRS4 cells, and LPS

Poly-ethylene-oxide-block-poly-butadiene (PEO-b-PBD) copolymers that formed cylindrical micelle nanoparticles (CNPs) and spherical micelle nanoparticles (SNPs) were synthesized according to the methods of Ref. 15. The PEO of the CNPs and SNPs is terminated with an -OH group, which is the terminal PEO chemistry used in Refs. 1, 13–15, 20, 17-. CNPs and SNPs were formed at 10 mg ml<sup>-1</sup> copolymer using film rehydration with phosphate buffered saline (PBS) as the aqueous buffer [18]. PEGylated lipid nanoparticles (PLs) are the shells of the anticancer nanoparticle, DOXIL, which were purchased pre-formed (FormuMax; #f30204b-c). PLs are comprised of HSPC:cholesterol:DSPE- $\mbox{PEG}_{2000}$  (mol: 56.2:38.5:5.3). The PEG of DSPE-PEG  $_{2000}$  of DOXIL is terminated with a methyl group. The studies in Refs. 5–7, 11, 16, 21 also used a PEGylated lipid with a methyl group at the end of the PEG. We use the acronym PEG to represent both PEG and PEO though their termini differ. Note that CNPs and SNPs have a 100% PEG exterior and 5% of the lipids in PLs are PEGylated (2000 g mol<sup>-1</sup> PEG). All NPs used in fluorescence microscopy and flow cytometry experiments were stained with ~50 nM of near-infrared (NIR) dve (Life Technologies; #D12731) [1,17]. The dye was added in five 10 nM aliquots and mixed thoroughly with the CNPs, SNPs, or PLs [22]. We kept the mass percent of the NIR dye to the amphiphile mass in each PEG-NP sample constant at  $\sim 0.5\%$ [1,16]. The molar ratios of amphiphile to NIR dye were  $\sim$  40:1 (CNP), ~24:1 (SNP), ~250:1 (PL). All PEG-NPs were dialyzed into PBS for 24 h after addition of NIR dye (14 kDa membrane). To test if NIR dye leaked from the PEG-NPs, we added the above amount of NIR dye to the PEG-NPs and dialyzed the labeled PEG-NPs in 100 ml of DMEM +10% FBS for 24 h. The NIR signal of CNPs, SNPs, and PLs was statistically equivalent before and after dialysis as measured in a Varioskan LUX plate reader (Fig. S1A-C). The diameters of CNPs, SNPs, and PLs did not change significantly after NIR addition as measured by dynamic light scattering (DLS) (Fig. S1D-F). These two results confirm that the NIR dye does not leak from the PEG-NPs, and that the NIR dye does not affect the sizes of the PEG-NPs. These results agree with previous work [1,17]. PEG-NPs were prepared for and imaged using scanning electron microscopy (SEM) using the techniques of Ref. 1. Human lipoproteins were purchased from Lee Biosolutions: hHDL (#361-10), hLDL (#360-10), oxLDL (#360-31), VLDL (#365-10), chylomicrons (#194-14). JRS4 cells were a gift from Dr. Michael Caparon (Washington University, St. Louis) and were cultured in Todd Hewitt broth (Fisher; #IFU64800). Lipopolysaccharide (LPS) was purchased from Sigma (#L2630).

### 2.2. Protein-NP binding, size-exclusion chromatography, protein-JRS4 binding, and proteomics

All mouse plasma, human serum, and protein samples were centrifuged at 15,000 xg for 15 min at 4 °C prior to use. We used the supernatant, which contains only soluble proteins, for binding experiments so that we would not have false positives in size-exclusion elution or in pull-down experiments involving JRS4 cells. For the experiments that determined the identities of mouse plasma proteins that bound PEG-NPs, fifty microliters of CNPs, SNPs, and PLs formed at 10 mg ml<sup>-1</sup> in PBS were dialyzed into DMEM. Each of these three PEG-NP samples was mixed with fifty microliters of mouse plasma pooled from three 12week-old C57BL/6 J female mice on a chow diet. For a control, fifty microliters of DMEM without PEG-NPs was mixed with the mouse plasma in equal volumes. The resulting four samples (100  $\mu l)$  were incubated separately for 15 min at 37 °C. The samples were run separately through agarose gel mini-columns (Cell Guidance Systems; #EX02-8). The volumes of the fractions coming out of the column were  $\sim 100$  µl. We collected the first five fractions. The total collection time was less than one minute.

For the experiments to determine the identities of human serum proteins that bind NPs, we performed the exact experiment as above but replaced mouse plasma with fifty microliters of human serum from a 62-year-old female donor: "hSerum" (Versiti, Inc.) (#IRB-20-06176-XP) and DMEM with human plasma-like medium (HPLM) (Thermo; #A4899101).

For the experiments to determine if human  $\gamma$ -globulin ( $\gamma G$ ) and complement bound PEG-NPs, fifty microliters of CNPs, SNPs, and PLs were formed at 10 mg ml $^{-1}$  in PBS and dialyzed into HPLM. Each PEG-NP was mixed separately with fifty microliters of combined 10 mg ml $^{-1}$   $\gamma G$  from human blood (Sigma; #G4386) dissolved in HPLM and 1 mg ml $^{-1}$  human complement (Pel-freez; #34010) also dissolved in HPLM.  $\gamma G$  are immunoglobulins and occur in five classes: IgG, IgM, IgA, IgD, and IgE. The resulting 100  $\mu l$  samples were incubated for 15 min at 37  $^{\circ}C$  and run separately through four mini-columns.

PEG on the PEG-NPs was in molar excess in each of the above experiments. Thus, the proteins could saturate the PEG-NPs. For each of the size-exclusion chromatography experiments, media (either DMEM or HPLM) was added to the column just as the experimental mixture completely entered the resin. For each of the above three experiments that determined the proteins bound to PEG-NPs, the eluted fractions were measured for absorbance at 280 nm (Fig. S1G) (Nanodrop). The presence of NPs of the correct size was measured using dynamic light scattering (DLS) on a N3700 Zetasizer Nano DLS Detector.

To determine the opsonization of proteins on a pathogen compared to opsonization of proteins on PEG-NPs, fifty microliters of JRS4 cells (O. D. ~1.0) were pelleted and resuspended in either DMEM (mouse proteins) or HPLM (human proteins) and mixed with fifty microliters each of the above mouse plasma, human serum, and  $\gamma$ -globulin + complement samples for 15 min at 37 °C. The mixtures were centrifuged at 10,000 xg for 15 min at 4 °C. The supernatant containing unbound proteins was removed and the pellet containing JRS4 cells and any bound proteins was washed with ice-cold PBS. The pellet, which should not contain any false positives because of our pre-experiment spins at higher velocities, was resuspended in 100 µl of PBS - the exact volume of the mixtures of CNPs + proteins, SNPs + proteins, and PLs + proteins. Relevant eluted fractions from the above three size-exclusion experiments (mouse plasma, human serum, and γ-globulin + complement) and the re-suspended JRS4 pellet were run on SDS-Page gels, which were stained with Coomassie Blue. Bands were extracted and the proteins were identified using mass spectrometry at the University of Tennessee Health Science Center - Memphis (Dr. David Kakhniashvili). Further details are in Supplemental Methods.

#### 2.3. CNP biodistribution in wild-type C57BL/6 J and NSG mice

All mouse protocols were approved by the University of Tennessee's IACUC (#2231). CNPs carrying NIR dye were tail-vein injected at 5 mg  $\rm kg^{-1}$  into nine C57BL/6 J (Jackson Laboratories; #000668) and nine NSG (Jackson Laboratories; #005557) mice. The mice were female and male. No differences in biodistribution were seen between the sexes. Forty-eight hours post injection, the mice were euthanized, the organs were harvested, and imaged on an IVIS system.

#### 2.4. Wild-type C57BL/6 J mouse vaccination and analysis

Five C57BL/6 J male mice were subcutaneously injected with 5 mg  ${\rm kg}^{-1}$  SNPs (no dye) at days 0, 14, and 28 (three injections total into each group) [23]. Blood was collected from the same mice at days 0, 14, 28, and 42. Each blood sample was analyzed for IgG, IgM, and IgA against PEG using ELISA (Enzo; #ADI-900-213-0001). The antibody in this kit binds the backbone of PEG. It is unknown how a single PEG molecule or PEG that is part of a NP is presented to a cell that produces antibodies. ELISA analysis was performed in technical triplicate for each of the five mice.

#### 2.5. Fluorescence microscopy and flow cytometry

We polarized all macrophages to a mild pro-inflammatory state by adding 10 ng  ${\rm ml}^{-1}$  IFN $\gamma$  (Sino; #50709-MNAH). IFN $\gamma$  is the main cytokine associated with M1 activation, the main Th1 cell product, and increases phagocytosis and oxidative burst [24].

THP-1 human-derived macrophages (ATCC; #TIB-202) were cultured in 96-well plates to confluence in HPLM with human serum from a 62-year-old female donor ("hSerum"). The THP-1 cells were washed three-times with PBS. Half the cells were incubated in HPLM +10% hSerum and the other half were incubated in HPLM only. CNPs, SNPs, and PLs that were carrying NIR dye were added to the wells at a final concentration of 800  $\mu g \ ml^{-1}$  for 2 h (8% of total media volume). The THP-1 cells were then analyzed by flow cytometry for NIR signal. THP-1 are suspension cells; thus, we did not collect fluorescence micrographs.

RAW264.7 mouse macrophages (ATCC; #TIB-71) were cultured in 96-well plates to confluence in DMEM +10% FBS  $+\ 1\%$  P—S. The RAW264.7 mouse macrophages were washed three-times with PBS. Half the cells were incubated in DMEM +10% FBS and the other half were incubated in DMEM only. CNPs, SNPs, and PLs that were carrying NIR dye were added to the wells at a final concentration of 800  $\mu g\ ml^{-1}$  for 2 h.

Mouse BMDMs were isolated from three-week-old BALB/c female mice. The monocytes were polarized to M0 macrophages and then to IFN $\gamma$ -polarized macrophages using standard protocols [25]. The PEG-NP incubation protocol was identical to that for the RAW264.7 mouse macrophages. Macrophage nuclei were identified using Hoechst (Enzo; #HOE33342).

#### 2.6. Lipoprotein and PEG-NP competition experiments

RAW264.7 mouse macrophages were cultured in 96-well plates to confluence in DMEM +10% FBS + 1% P—S. The RAW264.7 mouse macrophages were washed three-times with PBS then incubated in DMEM. Lipoproteins were then added to the wells for 15 min in the following concentrations: hHDL (2.5 mg ml $^{-1}$ ) [1], hLDL (2.5 mg ml $^{-1}$ ) [1], oxLDL (2.5 mg ml $^{-1}$ ), VLDL (2.5 mg ml $^{-1}$ ), chylomicrons (2.5 mg ml $^{-1}$ ). After 15 min, CNPs (800  $\mu$ g ml $^{-1}$ ), SNPs (800  $\mu$ g ml $^{-1}$ ), and PLs (800  $\mu$ g ml $^{-1}$ ) carrying NIR dye were added to the wells. After two hours, the macrophages were washed with PBS and imaged for NIR signal using fluorescence microscopy. The macrophages were then trypsin digested (100  $\mu$ l) for 5 min at 37 °C and mixed with ice-cold 0.5% BSA in PBS (100  $\mu$ l). The NIR signals of the suspended macrophages,

representing the uptake of PEG-NPs, were analyzed using flow cytometry (CytoFLEX V0-B3-R1) in biological triplicate.

#### 2.7. RNA sequencing and analysis

We performed two bulk mRNA sequencing experiments. In the first, RAW264.7 mouse macrophages were incubated in DMEM +10% FBS with the following reagents for 24 h: hHDL (200  $\mu g$  ml $^{-1}$ ), hLDL (200  $\mu g$  ml $^{-1}$ ), PL (200  $\mu g$  ml $^{-1}$ ), LPS (100 ng ml $^{-1}$ ), and PBS (2% by volume). JRS4 cells (MOI  $\sim$  50) were incubated with the RAW264.7 mouse macrophages for 3 h. In the second sequencing experiment, BALB/c BMDMs were incubated in RPMI +10% FBS with the following reagents for 2 h: hHDL (800  $\mu g$  ml $^{-1}$ ), SNP (800  $\mu g$  ml $^{-1}$ ), and PBS (8% by volume). No dye was used in these experiments. mRNA was isolated from all macrophages (Zymo; #R2050). mRNA from the RAW264.7 mouse macrophages was sequenced at BGI, Inc. Reads were analyzed using the BGI suite: "Dr. Tom". PCA and Pearson's coefficients were calculated by BGI. mRNA from the BMDMs was sequenced and analyzed at UTK.

#### 2.8. Measurement of autophagosomes

All experiments were performed on RAW264.7 mouse macrophages. The final concentrations of hHDL, hLDL, PEG, CNPs, SNPs, and PLs were 200  $\mu g$  ml $^{-1}$ ; thus, the mass of material was consistent throughout these experiments. We chose 24 h as our analysis timepoint for all reagents except JRS4 cells (3 h) [26]. JRS4 cells (MOI  $\sim$  50) were identified with the DNA marker TOTO $^{\rm IM}$ -3 iodide 642/660 (Thermo; #T3604). Rapamycin was added to a final concentration of 250 nM. LPS (Sigma; #L2630) was added to a final concentration of 100 ng ml $^{-1}$  [27]. After the incubation times, macrophages were washed with PBS then stained for 10 min with a proprietary green fluorescence kit CYTO-ID (Enzo; #ENZ-KIT175). The macrophages were washed again with PBS and imaged on a fluorescence microscope (EVOS). After imaging, the macrophages were trypsinized (100  $\mu$ l) for 5 min at 37 °C. After incubation, the macrophages were removed from the well by gentle pipetting. They

were then added to an equal volume of ice-cold 0.5% BSA in PBS. Samples were run in biological triplicate on an Accuri C6. Doublets were eliminated by their position in the FSC-H vs. FSC-A plot. We used FIJI for image analysis, and FCS Express 7 Research Edition and FlowJo for flow cytometry gating. *p*-values for flow cytometry data were determined using the Excel t.test() function.

#### 2.9. Cytokine and chemokine panels

CNPs (200  $\mu g \ ml^{-1}$ ), SNPs (200  $\mu g \ ml^{-1}$ ), PLs (200  $\mu g \ ml^{-1}$ ), LPS (100  $ng \ ml^{-1}$ ), and PBS (2% by volume) were incubated with RAW264.7 mouse macrophages in DMEM +10% FBS for 24 h. The resulting media was collected, centrifuged to eliminate any cells or cell debris, and analyzed for cytokines and chemokines (Eve Technologies; #MD32).

#### 3. Results

#### 3.1. General NP properties

We aimed to determine how PEG-based cylindrical micelle nanoparticles (CNPs), PEG-based spherical micelle NPs (SNPs), and PEGylated liposome NPs (PLs) bind and affect macrophage physiology. The CNPs and SNPs used in this study had a 100 mol% PEG exterior and a polybutadiene (PBD) interior (Fig. 1A). The PLs were formed from the bilayer components of the anti-cancer NP, DOXIL, without doxorubicin (Fig. 1B). Five mole percent of the PL constituents were PEGylated (DSPE-PEG<sub>2000</sub>). Schematic diagrams of CNPs, SNPs, and PLs are shown in Fig. 1C. All three PEG-NPs are stable in PBS and in standard macrophage cell culture media: DMEM +10% FBS (Fig. 1D). To determine the effects of these PEG-NPs on macrophage viability, we incubated free PEG2k, CNPs, SNPs, PLs, and chloroquine (CQ) with RAW264.7 mouse macrophages for 24 h. Chloroquine was used as a control for halting cell division. None of the PEG-NPs halted RAW264.7 mouse macrophage division (Fig. S2A). Thus, PEG-NPs do not appear to be toxic in this in vitro environment as measured by the proliferation of immortalize macrophages.

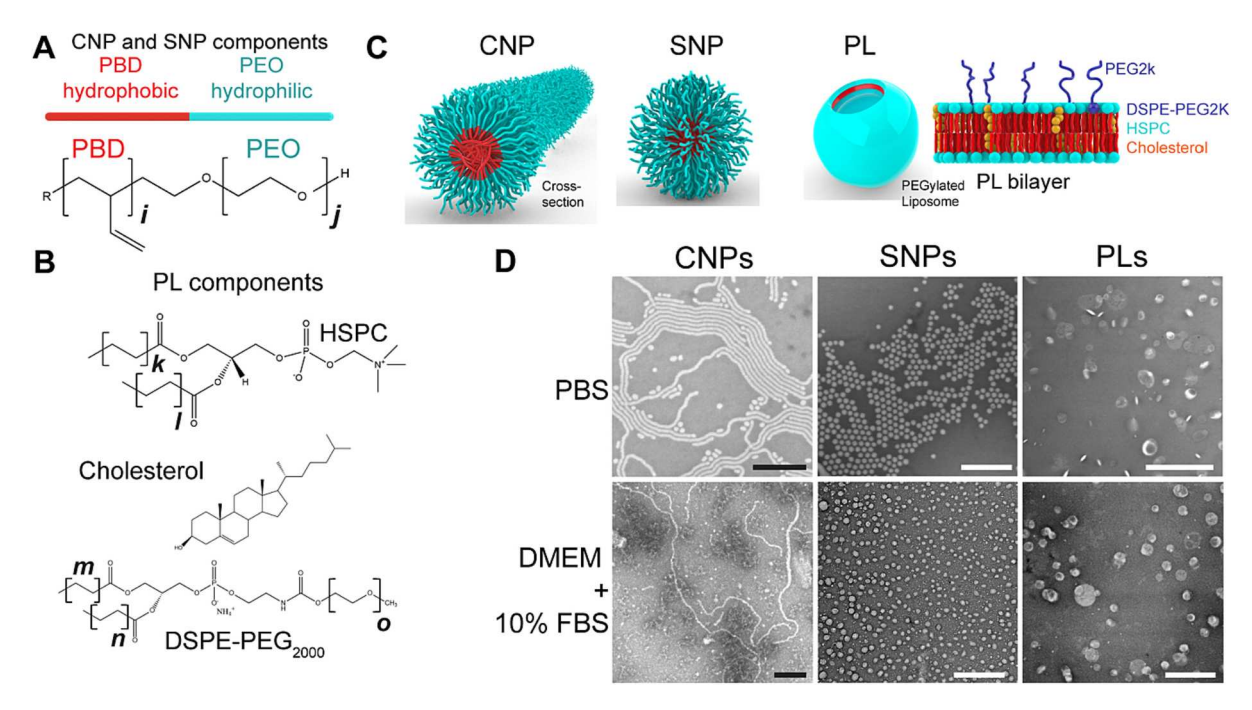


**Fig. 1.** Properties of the nanoparticles (NPs) used in this study. (A) Chemistries of the components of CNP and SNP micelles. For the CNPs: i = 46, j = 56. For the SNPs: i = 69, j = 132. (B) PLs are assembled from HSPC:cholesterol:DSPE-PEG<sub>2000</sub> (56.2: 38.5: 5.3 mol). For the PLs: k = 8 and l = 8, m = 8 and n = 8, and o = 45. (C) Schematic drawings of the three PEG-NPs used in this study. Drawings are not to scale: a one-micron-long CNP has  $\sim 1$  M copolymers, a 50 nm SNP has  $\sim 30$  k copolymers, and a 100 nm PL has  $\sim 85$  k lipids. (D) Electron micrographs of the CNPs, SNPs, and PL used in this study. CNPs, SNPs, and PL were incubated in PBS (top panels) or in DMEM +10% FBS for 3 h (bottom panels). Scale bars in (D) are 500 nm.

### 3.2. C57BL/6 J mouse plasma proteins have low affinity for CNPs, SNPs, and PLs compared to their affinity for JRS4 cells

To determine the mouse protein corona of CNPs, SNPs, and PLs, we split C57BL/6 J mouse plasma (mPlasma) into four 50 µl aliquots and mixed each with 50 µl of (1) DMEM, (2) CNPs, (3) SNPs, and (4) PLs for 15 min at 37 °C. We applied each of the four mixtures to four different size-exclusion chromatograph columns where large PEG-NPs with any bound plasma protein should elute before small free/unbound plasma protein. We collected fractions one minute after adding the mixtures to the columns. We used absorbance ( $\lambda 280$ ) and DLS to determine the presence of PEG-NPs and protein in each eluted fraction (Fig. S1G; Fig. S3A). No detectable protein or PEG-NP eluted in the first fraction (Fig. 2A). PEG-NPs, especially CNPs, began to elute in the second fractions (Fig. 2A). The protein signal stayed comparatively constant with its value in the first fraction (Fig. 2A). Any protein that had affinity for PEG-NPs should have bound PEG-NPs and eluted with the large PEG-NPs in the second fraction. If there was significant affinity between mPlasma and PEG-NP, much of the mPlasma that eluted in fractions 3-5 should have eluted in fraction 2 with the PEG-NP with which it was pre-mixed. This binding would have been reflected in the summation of the mPlasma (red) columns in fractions 3-5 to the CNP (orange), SNP (green), and PL (blue) columns in fraction 2 (Fig. 2A). To determine the identity of proteins that may have bound PEG-NPs, we performed mass spectrometry on the second fractions of the above four mixtures. The DMEM + mPlasma sample had  $\sim$ 70 proteins (Table S1). These proteins are represented by the small red column in Fig. 2A for the second fraction. The CNP + mPlasma sample had many of the same proteins as those in the PBS + mPlasma sample (Table S2). Of the proteins present in both samples, Ig heavy constant mu, ApoA-II, C1q, complement factor H, and Ig kappa chain V-III were enriched in the CNP + mPlasma sample (Table S3). ApoB-100, complement C3, ApoA-IV, ApoA-I, and Ig heavy chain V-III were depleted in the CNP + mPlasma sample (Tables S1-3). Thus, we did not observe a trend in immunoglobulin, complement, or apolipoprotein binding to CNPs. The proteins in the SNP + mPlasma and PL + mPlasma second fractions were too sparse to be reported with confidence, though SNP and PL had  $\lambda$ 280 signal (Fig. 2A). Therefore, mPlasma proteins have negligible affinity for SNPs and PLs as measured by size exclusion chromatography and mass spectrometry.

As a positive control for a foreign particle for which plasma proteins have affinity, we used group A *Streptococcus* JRS4 cells. JRS4 cells are too large for size-exclusion chromatography but can be separated from unbound proteins using low speed centrifugation. We mixed JRS4 cells with mPlasma for 15 min at 37  $^{\circ}$ C, pelleted the JRS4-protein mixture at 10,000 x g for 15 min, gently washed the JRS4 cells in the pellet with PBS, and resuspended the pellet with fresh PBS. In contrast to the sparse protein coronas of the PEG-NPs, ~230 proteins pelleted with the JRS4 cells (Table S4). These proteins included apolipoproteins, complement,

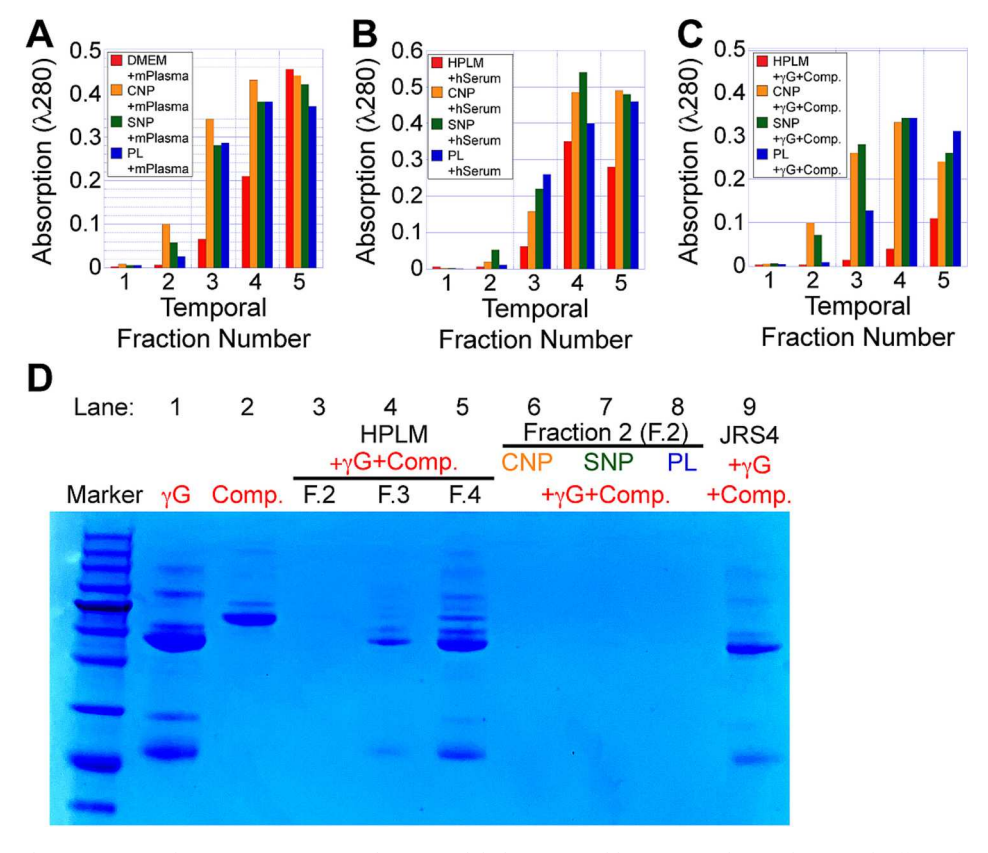


Fig. 2. Mouse plasma (mPlasma) proteins, human serum proteins, human  $\gamma$ -globulin ( $\gamma$ G), and human complement have weak affinity for PEG-NPs. (A) Plot of the absorbance ( $\lambda$ 280) of the first five eluted fractions of four separate mixtures of (1) DMEM + mPlasma, (2) CNP + mPlasma, (3) SNP + mPlasma, or (4) PL + mPlasma that were added to an Exo-spin column. Largest particles elute first in this technique: PEG-NPs (especially CNPs) elute before the majority of the DMEM + plasma in fraction 2 (orange v. red). Each of the five fractions had a volume of  $\sim$ 100  $\mu$ L. (B) Plot of the absorbance ( $\lambda$ 280) of the first five eluted fractions of four separate mixtures of (1) HPLM + human serum, (2) CNP + human serum, (3) SNP + human serum, and (4) PL + human serum that were added to an Exo-spin column. (C) Plot of the protein absorbance ( $\lambda$ 280) of the first five fractions of four separate mixtures that eluted from the Exo-spin column that was loaded with (1) HPLM +  $\gamma$ G + complement, (2) CNP +  $\gamma$ G + complement, (3) SNP +  $\gamma$ G + complement, or (4) PL +  $\gamma$ G + complement (four separate samples). (D) SDS-Page gel of (1)  $\gamma$ G, (2) complement, (3–5) the second, third, and fourth fractions eluted from the column to which HPLM +  $\gamma$ G + complement was added. (6–8) The second fractions eluted from the column when each indicated PEG-NP was incubated with  $\gamma$ G + complement before addition to the column. If  $\gamma$ G and complement bound the PEG-NPs, lanes 6–8 would look like lanes 4 and 5. (9) Resuspension of the pellet of the mixture of JRS4 cells +  $\gamma$ G + complement. (For interpretation of the references to colour in this figure legend, the reader is referred to the web version of this article.)

and immunoglobulins. Note, that we pelleted the plasma before adding it to any of the PEG-NPs or JRS4 cells and used only the supernatant in experiments. Thus, the proteins that pelleted with JRS4 cells should be in the pellet only because of affinity for JRS4 cells. These results show that mouse plasma proteins have weak affinity for CNPs, SNPs, and PLs as analyzed by size-exclusion chromatography.

### 3.3. Human serum proteins are not enriched on CNPs, SNPs, or PLs, but do bind JRS4 cells

We performed the same binding experiments but replaced mouse plasma with human serum from a 62-year-old female donor ("hSerum"). Here, the four mixtures were (1) HPLM + hSerum, (2) CNP + hSerum, (3) SNP + hSerum, and (4) PL + hSerum. As in the above experiments, after the incubation period, the PEG-NPs started eluting in the second fraction (Fig. 2B; Fig. S3B). The human serum proteins in the three PEG-NP second fractions and those in the HPLM + hSerum second fraction were similar (Tables S5-8). Thus, hSerum proteins were not enriched on PEG-NPs. On the other hand, complement, immunoglobulins, and apolipoproteins had a significant presence in the JRS4 cell pellet (Table S9). The amount of human serum added to all PEG-NP and JRS4 samples was equivalent. The PEG on the PEG-NPs was in molar excess to the proteins in the serum; therefore, all of the protein in the serum should bind PEG-NPs if significant affinity of the proteins for PEG on the PEG-NP exists. Instead, the signals of the proteins in the PEG-NP second fractions were 10-fold lower than those in the JRS4 cells. Thus, we conclude that the affinity of human serum proteins is much greater for JRS4 cells then for PEG-NPs.

### 3.4. Immunoglobulins and complement from human adults are not enriched on CNPs, SNPs, or PLs, but do bind JRS4 cells

We next focused solely on the affinity of human immunoglobulin and complement for PEG-NPs and JRS4 cells. We incubated (1) HPLM (control), (2) CNPs, (3) SNPs, and (4) PLs, with both 10 mg ml<sup>-1</sup> human  $\gamma$ -globulin ( $\gamma$ G) and 1 mg ml<sup>-1</sup> complete human complement. We ran the (1) HPLM +  $\gamma$ G + complement, (2) CNP +  $\gamma$ G + complement, (3) SNP +  $\gamma G$  + complement, and (4) PL +  $\gamma G$  + complement mixtures through size-exclusion columns for less than one minute and separated the eluent into  ${\sim}100~\mu l$  fractions, exactly as in the experiments with mouse plasma and human serum. The PEG-NPs, with any potential bound  $\gamma G$  and/or complement, began to elute in the second fraction (Fig. 2C; Fig. S3C). As above, we pelleted the JRS4  $+ \gamma G +$  complement mixture, gently washed the JRS4 cells in the pellet with PBS and resuspended the pellet with fresh PBS. We ran separate samples of pure γG (lane 1), pure complement (lane 2), the second-through-fourth eluent fractions of the HPLM  $\pm$  $\gamma G$  + complement mixture (lanes 3–5), the second fractions of the CNP  $+ \gamma G$  + complement mixture (lane 6), the SNP +  $\gamma G$  + complement mixture (lane 7), the PL +  $\gamma$ G + complement mixture (lane 8), and the resuspended JRS4 cell pellet (lane 9) on an SDS-Page gel to determine if  $\gamma G$  + complement bound NPs and JRS4 cells (Fig. 2D). HPLM +  $\gamma G$  + complement (without PEG-NPs) began to elute in the third fraction. The second fractions of PEG-NP  $+ \gamma G +$  complement mixtures had no bands (Fig. 2D). This implies that adult human  $\gamma G$  and complement have little to no affinity for these PEG-NPs. These experiments agree with the ones above where hSerum proteins were not enriched on PEG-NPs. The JRS4 lane had significant populations of proteins showing that these pathogens are opsonized. The affinity of γG and complement for JRS4 cells shows that  $\gamma G$  and complement are soluble and active in this experiment. The above three experiments show that (1) plasma proteins from mice that have not been exposed to PEG, PEG-NPs, or JRS4 cells have low affinity for CNPs, SNPs, and PLs, but high affinity for JRS4 cells, (2) adult (62-year-old) human serum proteins have low affinity for CNPs, SNPs, and PLs, but high affinity for JRS4 cells, and (3) adult human γG + complement have low affinity for CNPs, SNPs, and PLs, but high affinity for JRS4 cells.

## 3.5. Pre-existing mouse immune response factors do not affect PEG-NP biodistribution nor do mice have robust antibody production to PEG after PEG-NP injection

To further explore the effects of immunoglobulins on PEG-NP interactions with cells, we performed in vivo experiments in NOD scid gamma (NSG) mice. NSG mice lack mature T cells, B cells, natural killer cells, and, most importantly, serum immunoglobulin is not detectable [28]. We tail-vein injected CNPs carrying NIR dye into 12-week-old NSG mice (n=9) and 12-week-old wild-type C57BL/6 J mice (n=9). Of the three PEG-NPs, we chose CNPs because they have the longest circulation times and are model NPs for biodistribution studies [19]. We sacrificed all mice 48 h post CNP injection, harvested the major organs, and imaged them for CNP NIR signal. There was no significant difference in CNP liver signal between C57BL/6 J and NSG mice (Fig. 3A-B). These results show that the immunoglobulins that are present in mice prior to PEG exposure do not significantly affect CNP biodistribution over 48 h. Thus, we postulate that the basal or pre-existing immune response system plays a minimal role in the rapid PEG-NP localization to the liver.

If the pre-existing mouse immune response system does not significantly affect CNP biodistribution, we asked whether mice have robust antibody production to PEG-NPs. We subcutaneously injected five 12week-old mice with SNPs at days 0, 14, and 28. We collected blood from the mice at days 0, 14, 28, and 42. We performed ELISA on the plasma to determine the production of IgG, IgM, and IgA. IgG levels stayed constant for 28 days and increased less than two-fold after 42 days (p = 0.035). IgM levels increased modestly over 28 days and spiked at 42 days with high variability among samples; IgA levels did not increase over the same time course (Fig. 3C). IgM is produced within a few days of foreign antigen exposure; thus, we see a lag in production. IgG is the strongest of the three responses and titers are typically produced one week after antigen exposure; thus, we see a lag in IgG production as well. These data indicate that SNPs appear to trigger a late and minimal antibody production program that is much slower than the localization of any PEG-NP to mouse liver macrophages [17,19]. The lack of antibody production to SNP, with its long PEG/PEO group (j = 132; 5.4 kDa), agrees with recent findings that similar-length PEGs do not trigger antibody responses in mice [29].

 $\ensuremath{\mathsf{CNPs}},\ensuremath{\mathsf{SNPs}},$  and  $\ensuremath{\mathsf{PLs}}$  bind human and mouse macrophages without serum proteins.

Even though human immunoglobulins and complement were not enriched in the PEG-NP elution fractions in size-exclusion chromatography experiments, we wished to determine if human serum containing immunoglobulins, complement, and apolipoproteins increased the binding of PEG-NPs to human macrophages. We cultured human THP-1 cells in either HPLM or HPLM +10% human serum from the 62-year-old female donor and added CNPs, SNPs, or PLs for 2 h. The PEG-NP signal in the macrophages higher in the absence of serum proteins than in the presence of serum proteins (Fig. 4A,B). These results show that serum proteins do not appear to bind and guide PEG-NPs to human macrophage receptors. Instead, the components of serum slightly block the binding of these PEG-NPs to macrophages.

We performed similar experiments with mouse macrophages. We incubated immortalized RAW264.7 mouse macrophages, and primary bone-marrow-derived mouse macrophages (BMDMs) in standard culture media for 24 h and then washed the macrophages three times with PBS and replaced the media with DMEM +10% FBS or DMEM only. We incubated either CNPs, SNPs, or PLs with the three sets of macrophages for 2 h. Macrophage CNP, SNP, and PL signals either increased or stayed constant in serum-free conditions over 10% FBS conditions for all three PEG-NPs for both macrophage cell lines (Fig. 4C-H; Fig. S4). These experiments confirm those above performed with human serum and human macrophages and show that these PEG-NPs can bind macrophages directly without serum proteins. Furthermore, serum proteins block and do not augment the PEG-NP signal in macrophages.

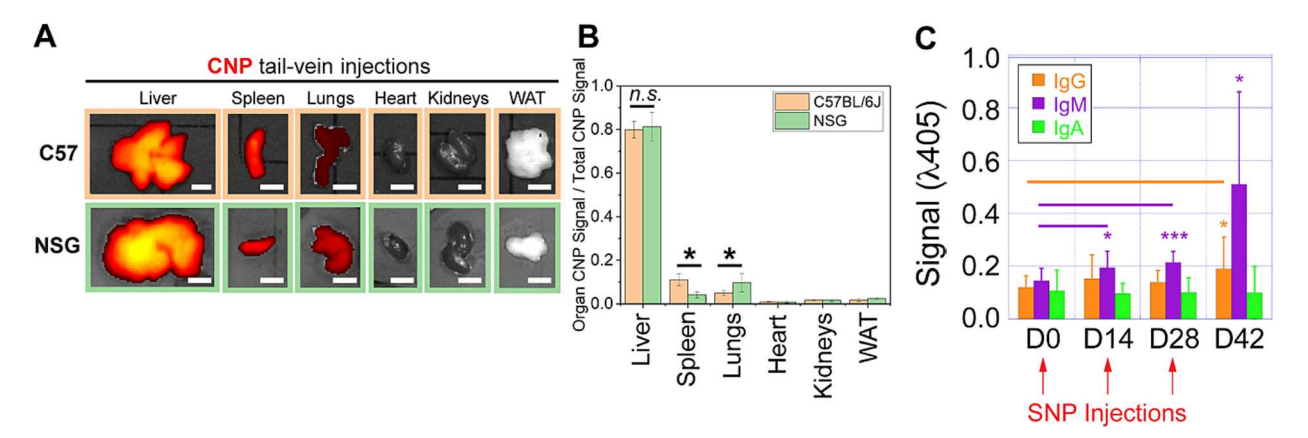


**Fig. 3.** Pre-existing mouse immunoglobulins do not affect CNP liver localization and SNPs trigger delayed and weak mouse immunoglobulin production. (A) Fluorescence images of the organs harvested from either C57BL/6 J (n=9) or NSG mice (n=9) 48 h post CNP injection. CNPs were carrying NIR dye. WAT is white adipose tissue. Scale bars are 5 mm. (B) Plot of the organ CNP signal divided by the total CNP signal of all the major organs shown in (A). (C) Plot of the indicated immunoglobulin levels in the isolated plasma of C57BL/6 J mice (n=5) that were subcutaneously injected with 5 mg kg<sup>-1</sup> SNPs at days 0, 14, and 28. \* p < 0.005; \*\*\* p < 0.01; \*\*\*\* p < 0.005.

### 3.6. Co-incubation of lipoproteins with CNPs, SNPs, and PLs significantly lowers PEG-NP signals in RAW264.7 mouse macrophages

To determine if PEG-NPs and lipoproteins compete for the same macrophage surface receptors [1], we performed co-incubation experiments of the major lipoproteins with CNPs, SNPs, and PLs. We incubated separately the major lipoproteins – chylomicrons, hHDL, hLDL, oxLDL, and VLDL – and the PEG-NPs with RAW264.7 mouse macrophages for 2 h. hHDL (binds SR-BI) and hLDL (binds LDLR) significantly lowered CNP, SNP, and PL signals in RAW264.7 mouse macrophages (Fig. 5A-C). Oxidized LDL (oxLDL) (binds SR-A/MSR1) also lowered CNP and PL signals in macrophages but had less of an effect on SNP signal. VLDL and chylomicrons had less of a blocking effect on CNPs and PLs. VLDL and chylomicrons had no effect on SNP signal in macrophages. These results show that lipoproteins and not immune response factors affect PEG-NP – macrophage interactions. It is probable that lipoproteins in the human serum and in the FBS lowered the PEG-NP signal in human and mouse macrophages (Fig. 4).

# 3.7. PLs trigger unique, yet minimal, mRNA transcript changes compared to hHDL, hLDL, JRS4 pathogens, and LPS after incubation with RAW264.7 mouse macrophages

We determined the mRNA transcripts of RAW264.7 mouse macrophages that were incubated with PBS, hHDL, hLDL, LPS, and PLs for 24 h and with JRS4 cells for 3 h (Fig. S5A). We chose PL - the shell of DOXIL as a model NP for mRNA analysis because it is currently used in the clinic. mRNA levels from the PBS control samples were used as the basis for fold change (FC) values. Only transcript changes with values of |FC| > 5 and Q-values <0.05 are presented. JRS4 pathogens (1018<sup>+</sup>,611<sup>-</sup>) and LPS (975<sup>+</sup>,525<sup>-</sup>) triggered the largest statistically significant FC values where "+" refers to increased transcript numbers and "-" refers to decreased transcript numbers (Fig. 6A; Tables S10-14). Thus, JRS4 cells increased the mRNA levels of 1018 transcripts by at least FC > 5 and lowered the mRNA levels of 611 transcripts by at least FC < 5. PLs (172<sup>+</sup>,151<sup>-</sup>) triggered significantly fewer changes than JRS4 cells or LPS. hHDL (302<sup>+</sup>,198<sup>-</sup>) and hLDL (346<sup>+</sup>,225<sup>-</sup>) triggered similar statistically significant FC values. Principal Component Analysis (PCA) values for macrophage transcripts affected by PBS, hHDL, hLDL, and PL treatments formed a cluster away from those affected by JRS4 and LPS treatments (Fig. 6B). Pearson coefficients were highest among PBS, hHDL, hLDL, and PLs (Fig. 6C). Bubble plot analysis and transcript per million (TPM) analysis are included in Supplemental Materials (Fig. S6-9).

### 3.8. SNPs and hHDL trigger similar mouse bone marrow-derived macrophage (BMDM) transcription programs

Given the results of the bulk mRNA sequencing of RAW264.7 mouse macrophages where the transcriptional response of macrophages to PBS, hHDL, hLDL, PL was different from that to LPS and JRS4 cells, we probed the transcriptional response of primary macrophages to hHDL and PEG-NPs. We incubated primary mouse BMDMs separately with PBS, hHDL, and SNPs in RPMI +10% FBS for two hours. The transcriptional response of BMDMs incubated with hHDL and SNPs formed a distinct cluster away from PBS-treated BMDMs (control) as measured by PCA (Fig. 7 A; Tables S15,S16) [30]. hHDL and SNPs both upregulated mRNA responsible for angiogenesis, cell migration, and extra-cellular matrix remodeling (GO classification) (Fig. 7B,C). hHDL and SNPs downregulated mRNA responsible for immune response, cytokine production, pattern recognition receptor signaling, and viral defense (GO classification) (Fig. 7B,C). Interestingly, hHDL upregulated mRNA involved in lysosome regulation (KEGG classification) (Fig. 7B; Table S17). Genes with the largest log<sub>2</sub>(FC) values from PBS controls were Atp6v0d2 (FChHLD-PBS ~ 2.5), Ctsk (FChHLD-PBS ~ 2.3), and Sort1 (FChHLD-PBS ~ 1.9). hHDL downregulated mRNA involved in viral infections, inflammasome, and TNF signaling (KEGG classification) (Fig. 7B). SNPs upregulated proliferation pathways, several metabolic pathways, and, interestingly, complement and coagulation cascades (Fig. 7C). Three of these twenty-two complement and coagulation genes are involved in complement binding: Cfh (FC<sub>SNP-PBS</sub> ~ 1.4), Itgam (FC<sub>SNP-PBS</sub> ~ 1.4), and Itgb2 (FC<sub>SNP-PBS</sub>  $\sim$  1.7) [31,32]. SNPs downregulated genes involved in immune response, cytokine production, and viral response factors (Fig. 7C). The KEGG pathways downregulated by SNPs matched those that were downregulated by hHDL (Fig. 7B,C). We mined the BMDM mRNA transcript data for genes involved in (1) cellular entry (modified CLEAR network) [33], (2) cytokine and chemokine production, and (3) autophagy. We plotted the genes from these categories in log<sub>2</sub>(FC) format (Fig. 7D-F). hHDL and SNPs increased Cd36 (Scarb3) which is typically associated with plasma fatty acid and oxLDL binding [34]. Cd36 is a co-receptor with Tlr4 and Tlr6 [35]. Thus, the increase in Tlr4 mRNA by hHDL and SNPs may coincide with the Cd36 increase, given that hHDL and SNPs did not increase toll-like receptor pathway factors in GO or KEGG analysis. hHDL and SNPs decreased Cd40 mRNA, the protein product of which is a member of the TNF-receptor family. hHDL and SNPs increased Cd163 mRNA, the protein product of which is a scavenger receptor involved in the anti-inflammatory response [36]. hHDL significantly increased Pdzk1 mRNA; SNPs slightly increased Pdzk1 mRNA (Fig. 7D). This is to be expected in a macrophage response

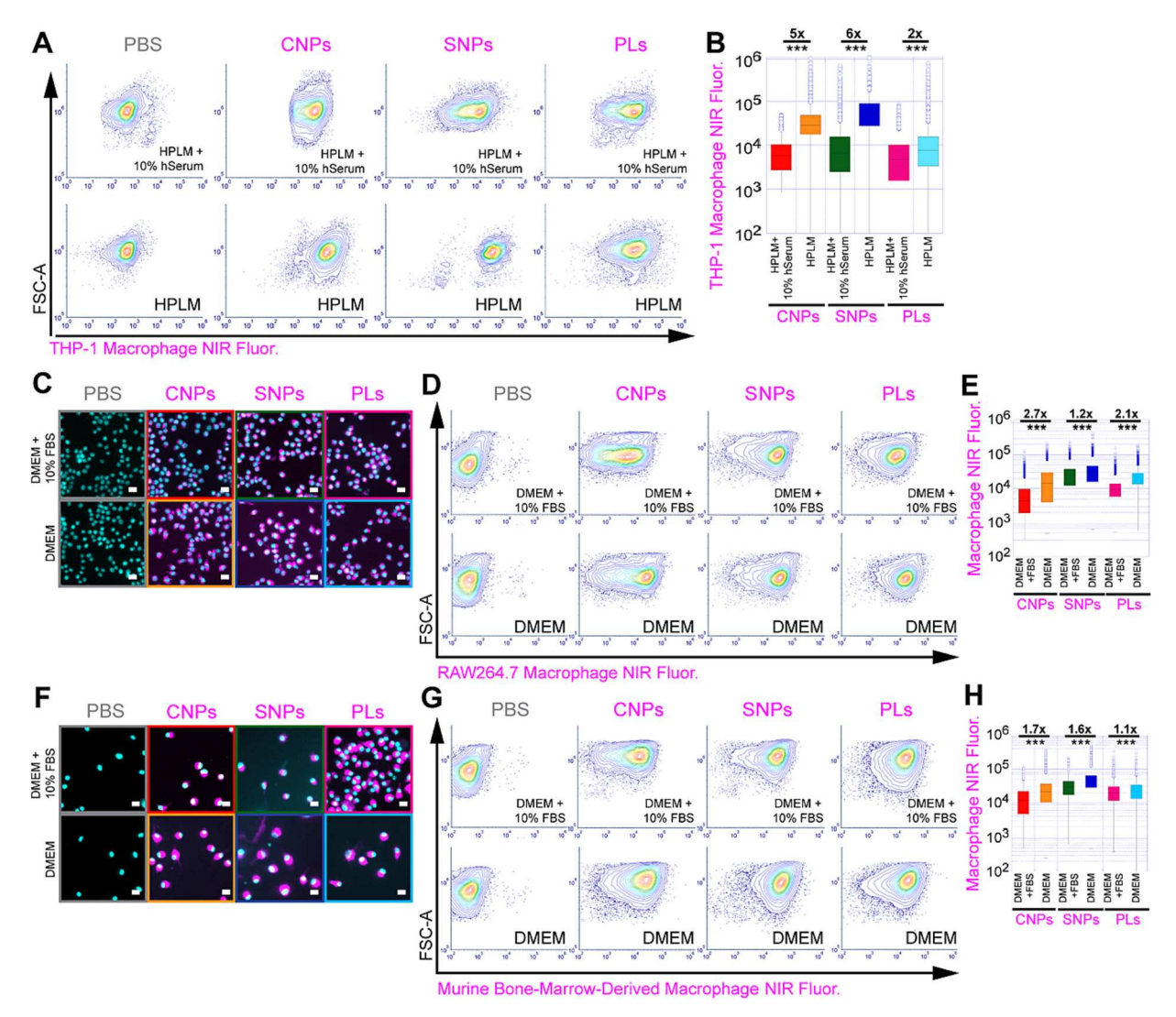


Fig. 4. PEG-NPs bind human and mouse macrophages without serum proteins. (A) Flow cytometry contour plots of THP-1 macrophages incubated with the indicated PEG-NPs carrying NIR dye in either HPLM +10% human serum (top row) or HPLM (bottom row). (B) Box plot of the flow cytometry data represented in (A). (C) Fluorescence micrographs of RAW264.7 mouse macrophages incubated with the indicated NPs carrying NIR dye in either DMEM +10% FBS media (top row) or DMEM media (bottom row). (D) Flow cytometry contour plots of the macrophages represented in (C). (E) Box plot of the flow cytometry data represented in (D). (F) Fluorescence micrographs of bone marrow derived macrophages incubated with the indicated NPs carrying NIR dye in either DMEM +10% FBS media (top row) or DMEM media (bottom row). (G) Flow cytometry contour plots of the macrophages represented in (F). (H) Box plot of the flow cytometry data represented in (G).  $n = 5000 \times 3$  (biological triplicate). \*\*\* p < 0.005.

to hHDL because Pdzk1 binds the cytosolic portion of SR-BI [37]. The mRNA changes of cytokine and chemokine factors from PBS controls were similar for hHDL and SNPs (Fig. 7E). Of note are the hHDL-modulated increases of Ccl2, Ccl7, and IL-6 mRNA. Of the genes involved in autophagy, hHDL and SNPs increased Ctsl, Mras, and Rras2 mRNA levels over PBS controls (Fig. 7F). Ctsl is a lysosomal proteinase; Mras and Rras2 activate the MAP kinase pathway [38]. From these data, we see that BMDMs respond similarly to hHDL and SNPs at the transcription level.

## 3.9. hHDL, hLDL, CNPs, SNPs, and PLs lower autophagosome levels in RAW264.7 mouse macrophages

NPs can trigger autophagy in mammalian cells [39]. To probe the effects of hHDL, hLDL, CNPs, SNPs, and PLs on autophagy, we incubated hHDL (carrying NIR dye) with RAW264.7 mouse macrophages for 24 h, washed the macrophages with PBS, and stained them with an autophagosome dye (CYTO-ID) (Fig. 8 A-C) [40]. The autophagosome signal dropped 60% compared to PBS controls as measured by flow cytometry of

CYTO-ID. We then used starvation / nutrient deprivation (DMEM without FBS), the mTOR inhibitor rapamycin (250 nM), or LPS (100 ng ml<sup>-1</sup>) to trigger autophagy. Starvation inhibits mTOR, which in turn activates autophagy. Rapamycin forms a complex with FK506-binding protein (FKBP12), which blocks mTORC1 kinase activity [41]. Since active mTOR inhibits autophagy, rapamycin triggers autophagy by this effect. LPS triggers autophagy so the cell can defend itself against invading pathogens. Each of these challenges caused the CYTO-ID signal to increase (Fig. 8A,C). hHDL lowered the CYTO-ID signal raised by each challenge (Fig. 8A,C). This shows that HDL has either anti-autophagosome formation properties or increases the flux of the autophagosome-lysosome merger. The second possibility is unlikely since hHDL did not increase the mRNA the lysosome biogenesis factor TFEB in either RAW264.7 mouse macrophages or BMDMs. We performed the same CYTO-IDlabeled autophagosome experiments with hLDL in place of hHDL and observed similar reductions in CYTO-ID signals (Fig. 8D-F). However, hLDL did not lower CYTO-ID signal as much as hHDL. In contrast to hHDL and hLDL, JRS4 cells labeled with the TOTO DNA dye increased the CYTO-ID signal in macrophages by 60% (Fig. 8G,H).

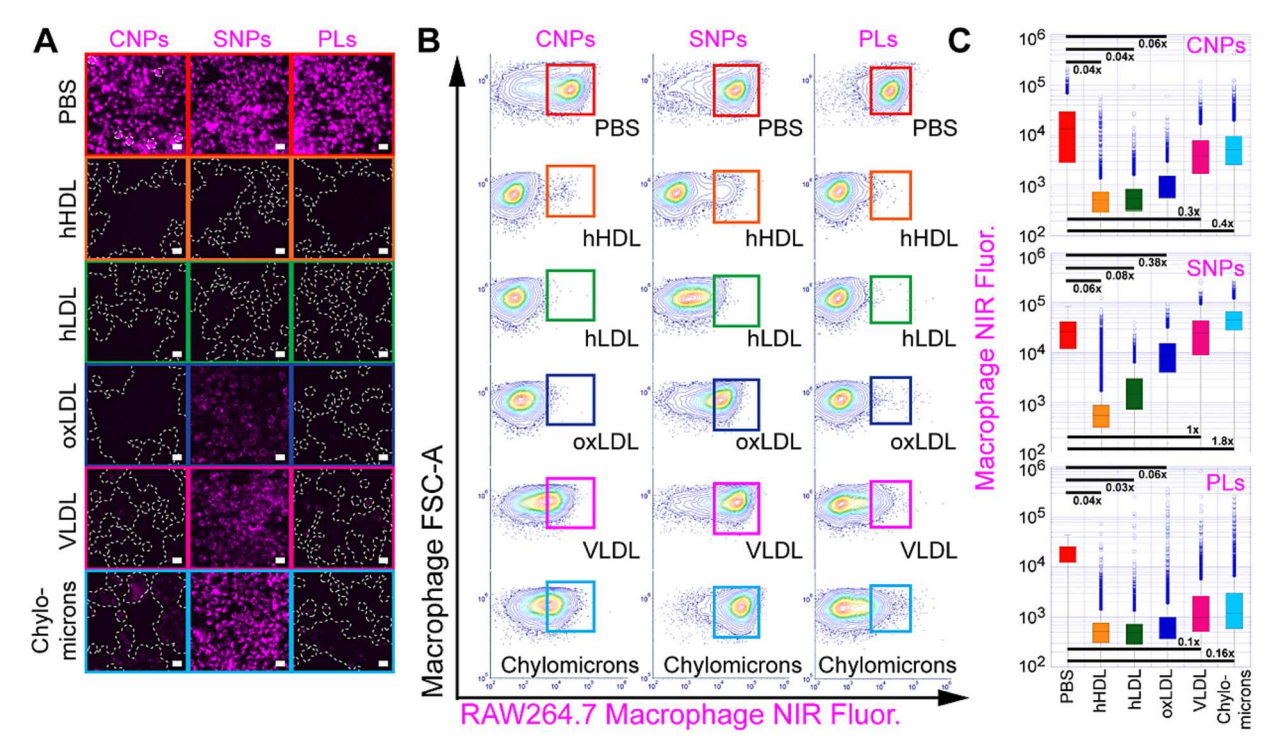


Fig. 5. Lipoproteins block the signal of PEG-NPs in RAW264.7 mouse macrophages. (A) Fluorescence micrographs of RAW264.7 mouse macrophages plated at confluence that were incubated with the indicated PEG-NP (carrying NIR dye) and the indicated lipoprotein in DMEM without serum. Dashed lines surround macrophages and are guides to the eye. Scale bars are 10  $\mu$ m. (B) Flow cytometry contour plots of the cells depicted in (A).  $n = 5000 \times 3$  (biological triplicate). (C) Box plots of the data in (B).

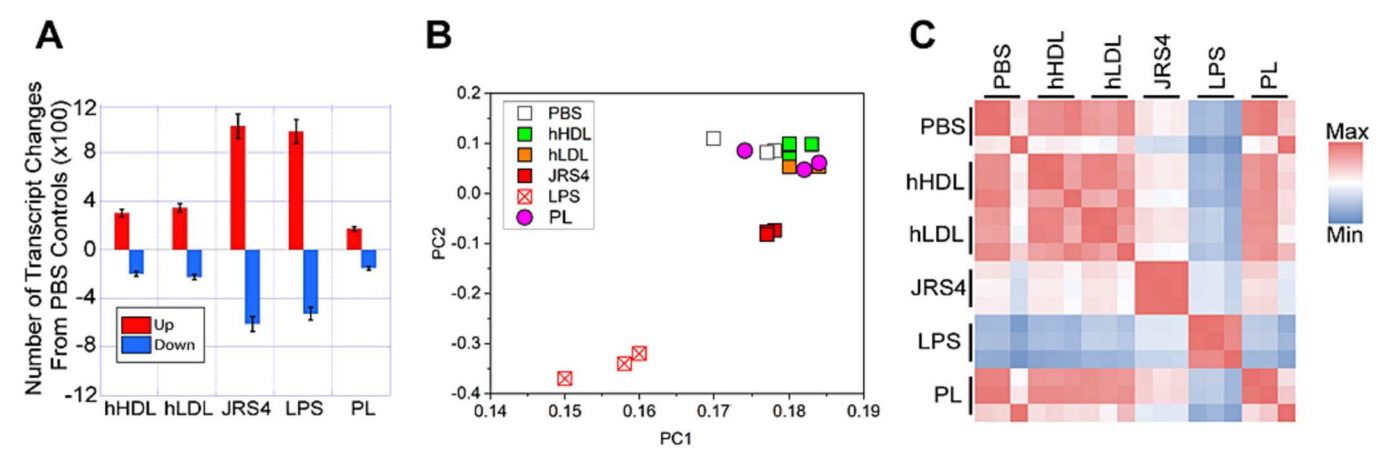


Fig. 6. JRS4 cells and LPS trigger significant changes in macrophage innate immunity and inflammation transcripts whereas hHDL, hLDL, and especially PLs trigger few changes in these pathways. (A) Plot of the number of macrophage transcripts that either increased (red) or decreased (blue) in a statistically valid manner (|FC| > 5 and Q-value <0.05) for each of the indicated treatments versus PBS controls. Incubation times were 24 h except for JRS4 cells (3 h). (B) Plot of the Principal Component Analysis (PCA) of macrophage transcripts after being incubated with the indicated reagents. (C) Plot of the Pearson coefficients of the macrophage transcripts after being incubated with the indicated reagents to colour in this figure legend, the reader is referred to the web version of this article.)

To determine the effects of our PEG-NPs on autophagosome abundance, we separately incubated PEG, CNPs, SNPs, and PLs with macrophages for 24 h in four different culture conditions: 1).

normal (DMEM +10% FBS), 2) starve (DMEM), 3) RAPA (250 nM rapamycin + DMEM +10% FBS), and 4) LPS (100 ng ml $^{-1}$  LPS + DMEM +10% FBS) [27]. We washed the macrophages in PBS and identified PEG-NPs using NIR dye. We identified autophagosomes with CYTO-ID using fluorescence microscopy and flow cytometry as in the experiments involving hHDL, hLDL, and JRS4 cells. Macrophage NIR signal (a measure of PEG-NP association) increased: PL > SNP > CNP (Fig. 9A-H). PEG slightly increased autophagosome signal (+20%) in DMEM +10% FBS.

conditions (Fig. 9I); on the other hand, SNPs and PLs reduced autophagosome signal, and CNPs had little effect, all in the same conditions (Fig. 9A,I). Neither PEG, CNPs, SNPs, nor PLs greatly affected autophagosome signal in starved conditions (Fig. 9B,J). CNPs, SNPs, and PLs reduced autophagosome signals by 30%, 50%, and 40% when coincubated with rapamycin (Fig. 9C,K). PEG increased the macrophage autophagosome signal by 20% when co-incubated with rapamycin. LPS significantly increased autophagosome signals over controls (Fig. 9I vs. 9 L, red boxes). However, PEG (-20%), CNPs (-50%), SNPs (-60%), and PLs (-40%) all lowered autophagosome signals raised by LPS (Fig. 9D,L). These results show that CNP, SNP, and PL but not PEG itself,

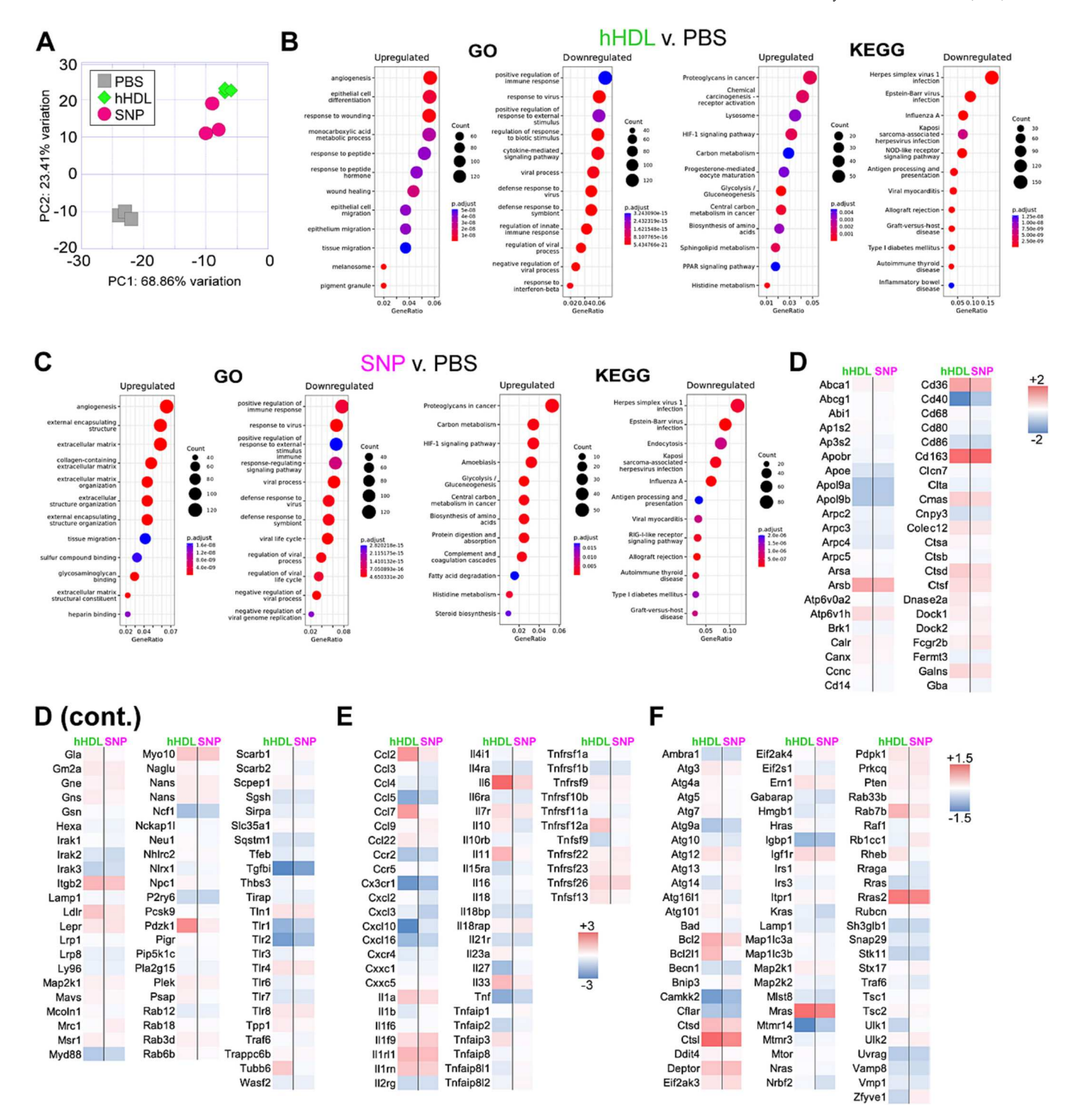


Fig. 7. hHDL and SNPs trigger highly similar mouse BMDMs transcriptome responses after two-hour incubations. (A) Plot of the Principal Component Analysis (PCA) of macrophage transcripts after being incubated with the indicated reagents. (B—C) Bubble plots of GO and KEGG enrichment pathways of macrophage mRNA transcripts after being incubated with the indicated reagents. (D—F) Heat maps of select genes that are involved in particle uptake (D), cytokine and chemokine production and secretion (E), and autophagy (F). Each rectangle is a value of log<sub>2</sub>(FC) with the mRNA level in BMDMs treated with PBS (equal volume to SNP buffer) as the baseline for the fold-change. All experiments were performed in biological triplicate.

can lower autophagosome levels as measured by CYTO-ID.

3.10. CNPs, SNPs, and PLs either lower or do not increase most cytokines and chemokines secreted by RAW264.7 mouse macrophages

To determine if macrophages secrete pro-inflammatory cytokines and chemokines in response to CNP, SNP, and PL binding, we collected

the media from each well of cultured RAW264.7 mouse macrophages after 24-h incubations with PBS, CNPs, SNPs, PLs, and LPS. We determined the levels of cytokines and chemokines by ELISA (Eve Technologies). We present only the cytokines and chemokines whose secretion levels were changed from PBS values by at least one of the NPs in a statistically significant manner (p-value <0.05). Unexpectedly, CNPs, SNPs, and PLs either lowered or did not increase the abundance of most

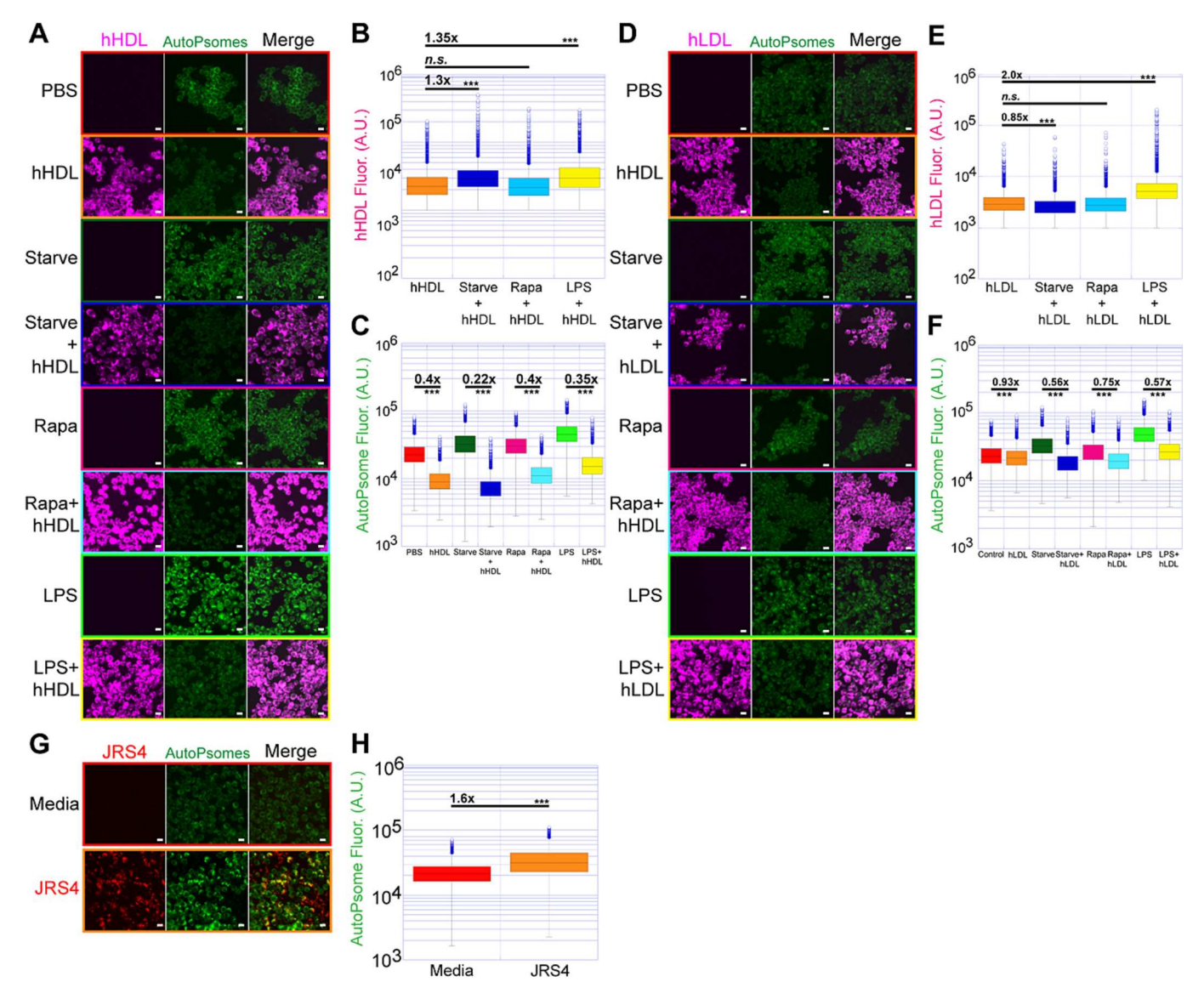


Fig. 8. hHDL and hLDL reduce autophagosome signals in RAW264.7 mouse macrophages. (A) Fluorescence micrographs of macrophages that have been incubated with the indicated reagents for 24 h subsequently stained with CYTO-ID to visualize autophagosomes. (B) Box plot of the intensity of the hHDL (NIR) signals of the macrophages depicted in (A) measured by flow cytometry. (C) Plot of the intensity of the autophagosome signals of the macrophages depicted in (A) measured by flow cytometry. (D) Fluorescence micrographs of macrophages that have been incubated with the indicated reagents for 24 h. (E) Plot of the intensity of the hHDL (NIR) signal of the macrophages depicted in (D) measured by flow cytometry. (F) Plot of the intensity of the autophagosome signal of the macrophages depicted in (D) measured by flow cytometry.  $N = 5000 \times 3$  (biological triplicate) for flow cytometry data. Scale bars are  $10 \mu m$ . \*\*\* p < 0.001.

cytokines or chemokines in the media after 24 h. Of the chemokines, a subset of CNPs, SNPs, and PLs significantly lowered the macrophage secretion of CCL2, CCL5, CXCL1, and CXCL9 (Fig. 10A-D); of the cytokines, a subset of CNPs, SNPs, and PLs significantly lowered the secretion of IL-1 $\alpha$ , IL-1 $\beta$ , IL-2, IL-6, IL-9, IL-10, IL-12p40, IL-13, IL-15, and IL-17 (Fig. 10F-O). A subset of CNPs, SNPs, and PLs also significantly lowered the macrophage secretion of G-CSF, M-CSF, TNFa, and VEGF (Fig. 10E,P-R). These results show that PEG NPs are capable of lowering macrophage cytokine and chemokine secretion and do not trigger a secretion profile that is similar to that triggered by the pro-inflammatory endotoxin LPS. In addition, JRS4 cells and LPS caused wide-spread increases in pro-inflammatory factor transcripts (Fig. 10S). On the other hand, hHDL, hLDL, and PLs triggered either no changes or reduced changes in cytokine, chemokine, and pro-inflammatory factor mRNA log<sub>2</sub>(FC) values. The notable exception was the increase in *Il1rl1* by hLDL. This member of the Tlr family does not induce an inflammatory response through activation of NF-κB but does activate MAP kinases. The reduction of inflammation by hHDL is to be expected [42].

 $SCARBI^{-/-}$  (the gene that codes for SR-BI) mice are hypersensitive to LPS [43]. LPS-induced cytokine expression in these animals was dependent on NF-κB, JNK, and p38. PEG and PEG-NPs bind SR-BI [1]. Therefore, a potential mechanism for inflammation inhibition by CNPs, SNPs, and PLs is their PEG-driven interaction with SR-BI (Fig. 11). Note that the reduction of cytokines and chemokines agrees with the mRNA transcript data when SNPs were incubated with mouse BMDMs for 2 h.

#### 4. Discussion

PEG-NPs begin localizing to mouse liver cells within minutes of entering the vasculature. The mice in which this rapid localization to the liver occurs are not exposed to PEG or PEG-NPs prior to injection [21]. Thus, the strong avidity of PEG-NPs for mouse liver cells should be independent of any immunoglobulins produced specifically against PEG or PEG-NPs. Pre-existing immunoglobulins produced by B cells against other moieties are the only options for antibody opsonization on PEG-NPs. Here, we showed that mouse plasma proteins - including

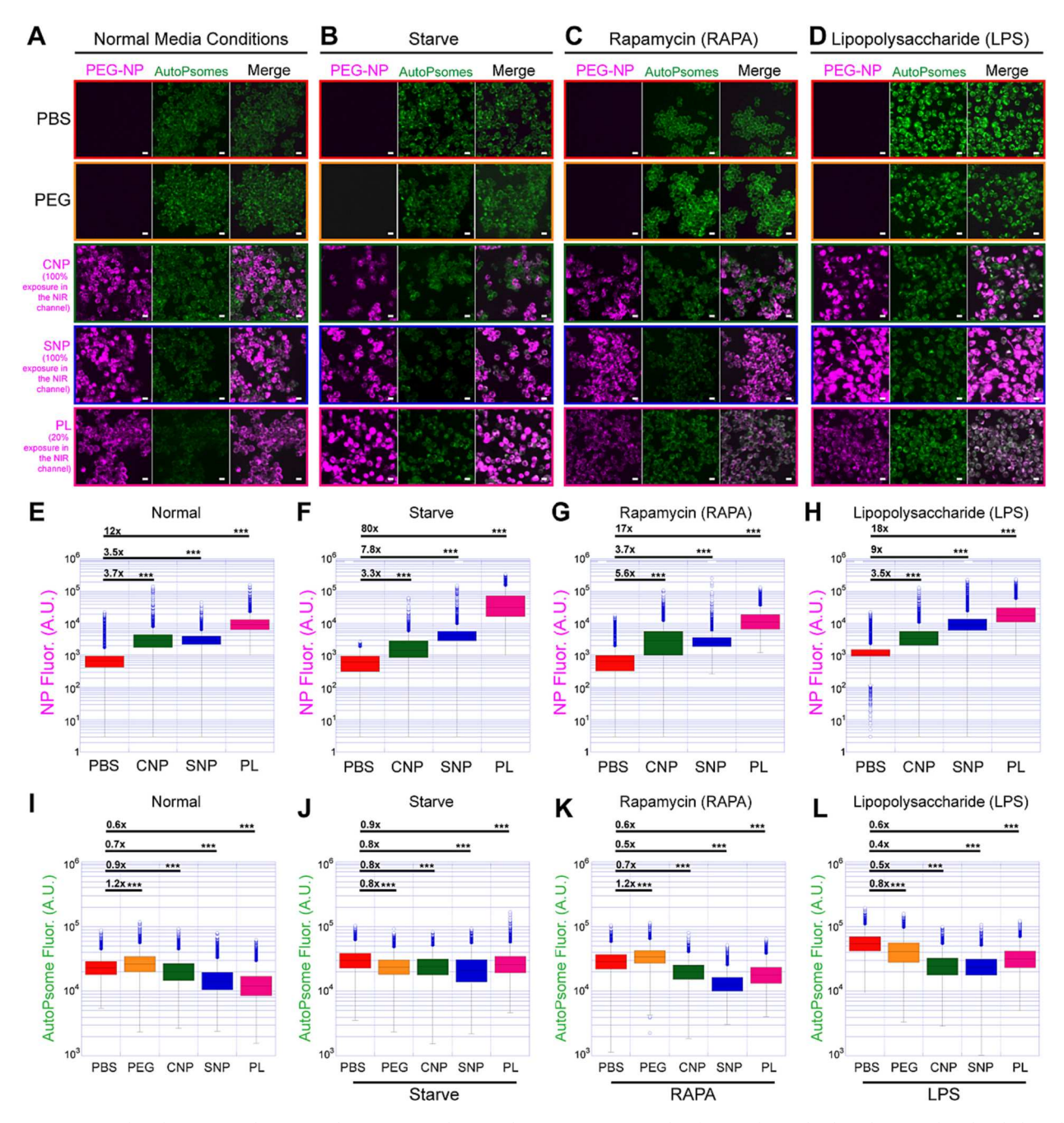


**Fig. 9.** CNPs, SNPs, and PL, but not PEG, lower autophagosome signal. (A-D) Fluorescence micrographs of macrophages that have been incubated with the indicated reagents for 24 h and subsequently stained with CYTO-ID to visualized autophagosomes. Scale bars are 10 μm. (*E*-H) Plots of the intensity of the NIR signal of the macrophages depicted in (A-D) measured by flow cytometry. (I-L) Plots of the intensity of the autophagosome signal of the macrophages depicted in (A-D) measured by flow cytometry.  $N = 5000 \times 3$  (biological triplicate) for flow cytometry data in (E-L). \*\*\*\* p < 0.001.

immunoglobulins and complement - had weak affinity for PEG-NPs. Our results showing that complement plays a weak role in PEG-NP binding to macrophages agrees with recent work showing that the complement cascade does not appear to be involved in in vivo clearance of PEG-NPs using a  $C3^{-/-}$  mouse [20]. SNPs triggered a weak IgG response and a delayed IgM response that were detected 42 days after the first of three SNP subcutaneous injections into mice. Furthermore, the biodistributions of CNPs in NSG mice and wild-type mice qualitatively matched. These in vivo results are in contrast to those showing that hHDL + CNP co-injections significantly lowered CNP liver localization in wild-type mice [1]. In the same study, CNP liver signal was significantly lowered in  $SCARB1^{-/-}$  mice (the gene that codes for SR-BI) over wild-type mice. In sum, it is doubtful that the mouse immune response

system plays a strong role in the rapid localization of PEG-NPs - with PEGylation greater than or equal to  $5\ mol\%$  - to the mouse liver.

We also showed that human serum proteins – including immuno-globulins and complement - had weak affinity for PEG-NPs. We showed that human serum from a middle-aged female did not augment the affinity of PEG-NPs for human macrophages as would be expected if the donor's immune system treated PEG as an antigen. These combined results discredit the first hypothesis that the immune response system is largely responsible for PEG-NP localization to the liver. However, unlike laboratory mice, it is possible that humans have antibodies against PEG because we have been exposed to PEG in cosmetics and soaps [21]. Also, the recent large-scale vaccination of humans with the Pfizer-BioNTech SARS-CoV-2 lipid nanoparticle (LNP) vaccine, which had a  $\sim 1{\text -}2$  mol

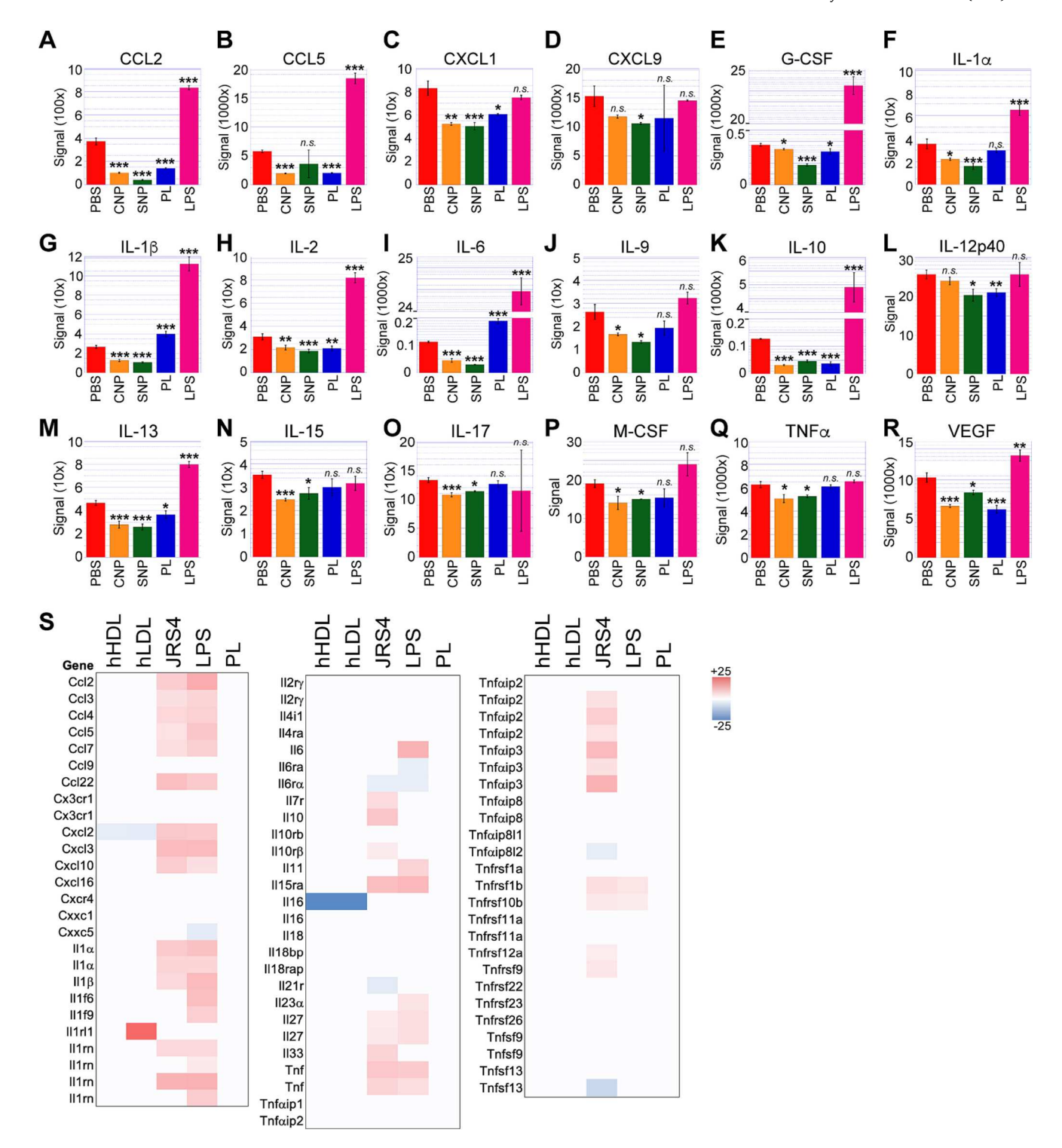


Fig. 10. CNPs, SNPs, and PL lower a significant number of cytokine or chemokine levels secreted by RAW264.7 mouse macrophages. (A-R) Plots of cytokine levels in the media of RAW264.7 mouse macrophages that were separately incubated with either PBS, CNPs, SNPs, PL, or LPS for 24 h. Each column represents three separate experiments. \* p < 0.05. \*\* p < 0.01. \*\*\* p < 0.005. (S) Heat map of RAW264.7 mouse macrophage mRNA transcripts whose protein products are important for innate immunity and inflammation. Repeated gene name entries are different isoforms.

% PEG component, could also cause the generation of antibodies to PEG and PEG-NPs [44]. A statistically expanded study where dozens of human serum samples are evaluated for the affinity of their proteins for PEG-NPs is needed.

Our findings also discredit the second hypothesis that apolipoproteins bind PEG-NPs and take them to lipoprotein receptors in the case of PEG-NPs with PEGylation of  $\geq$ 5 mol%. In our experiments,

apolipoproteins did not have appreciable affinity for the PEG-NPs used in this study. Instead, lipoproteins blocked and did not augment the association of our PEG-NPs for RAW264.7 mouse macrophages and BMDMs. We did not test LNPs where the PEGylation is  $\sim 1-2$  mol%. The lower the amount of PEG on the LNP, the stronger the affinity of apolipoproteins like ApoE should be for the exposed lipid head groups of the LNP [9,10]. The affinity of apolipoproteins for LNPs and the affinity of

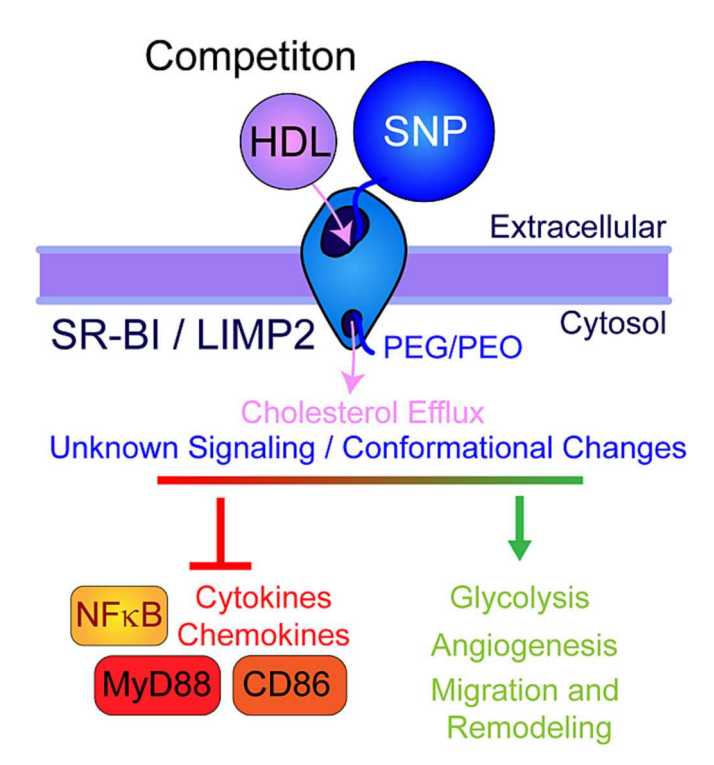


Fig. 11. Model of the competition between lipoproteins and PEG-NPs for macrophage receptor binding sites. In this model we chose HDL as the lipoprotein and SNPs as the PEG-NP. HDL binds SR-BI and LIMP-2 causing the transfer of HDL-cholesterol through the cholesterol tunnel. Cholesterol efflux into macrophages triggers inhibition of NFkB, inhibition of the toll-like receptor (TLR) adaptor protein MyD88, and down-regulation of the macrophage proinflammatory activation marker CD86. NFkB inhibition curtails the expression of pro-inflammatory cytokines and chemokines. HDL also triggers glycolysis, angiogenesis, cell migration, and extra-cellular matrix remodeling. Remarkably, SNPs (and possibly CNPs and PLs depending on the mole percent of PEG on the PL) trigger these same pathways in macrophages. It is mechanistically unknown how HDL and SNP binding to SR-BI and/or LIMP-2 cause similar macrophage responses.

the PEG on LNPs for cellular receptors would appear to be competing factors. If the former dominates, we anticipate that LNPs will bind LDLR; if the latter dominates, we anticipate that LNPs will bind PEG receptors such as the CD36 family of receptors: CD36, SR-BI, and LIMP-2. The pathway LNP trigger by binding either class of receptors could be a larger determinant in the efficacy of PLs and LNPs. Experiments that determine the effects of the transient presence of PEG on the surface of a general NP will help elucidate the trade-off between PEG binding cell surface receptors, versus adsorbed apolipoproteins guiding a general NP to apolipoprotein receptors [10,11]. A further restriction of our study is that we used a linear PEG moiety on our NPs. PEG branching and stacking can greatly affect biodistribution [45].

Our data indicate that PEG-NP interactions with macrophages are closer to lipoprotein-macrophage interactions than to pathogen-macrophage interactions. Our data show that direct interaction of the PEG component of PEG-NPs with receptors that bind apolipoproteins is most likely the key interaction between PEG-NPs and macrophages [1,13]. These results add validity to the third hypothesis. Recent work has identified other scavenger receptors, such as MARCO, as being important for PEG-NP biodistribution [12]. More work is needed to the identity of the receptors PEG and PEG-NPs bind and the affinity with which PEG and PEG-NPs bind these receptors.

#### CRediT authorship contribution statement

Monireh Asoudeh: Writing - review & editing, Writing - original

draft, Methodology, Investigation, Formal analysis. Nicole Nguyen: Writing – review & editing, Writing – original draft, Methodology, Investigation, Formal analysis. Mitch Raith: Methodology, Investigation, Conceptualization. Desiree S. Denman: Methodology. Uche C. Anozie: Methodology. Mahshid Mokhtarnejad: Methodology, Investigation. Bamin Khomami: Funding acquisition. Kaitlyn M. Skotty: Methodology, Investigation. Sami Isaac: Methodology, Investigation. Taylor Gebhart: Methodology, Investigation. Lauren Vaigneur: Methodology, Investigation. Aga Gelgie: Methodology, Investigation. Oudessa Kerro Dego: Methodology, Funding acquisition, Conceptualization. Trevor Freeman: Methodology, Investigation. Jon Beever: Methodology, Investigation, Funding acquisition. Paul Dalhaimer: Writing – review & editing, Writing – original draft, Project administration, Methodology, Investigation, Funding acquisition, Formal analysis, Conceptualization.

#### Data availability

The RNA-seq FASTQ files for bone-marrow-derived macrophages that were incubated with PBS, hHDL, or SNPs are available at GEO under accession GSE249596.

#### Acknowledgements

Research reported in this publication was supported by the National Institute Of General Medical Sciences under Award Number 1R15GM116037, the National Institute Of General Medical Sciences under Award Number T32 Integrated Membrane Program, and the National Institute Of Environmental Health Sciences of the National Institutes of Health under Award Number R25ES028976. The content is solely the responsibility of the authors and does not necessarily represent the official views of the National Institutes of Health. We thank Dr. Michael Caparon (Washington University, St. Louis) for JRS4 cells. We thank Dr. Frank S. Bates (University of Minnesota) for the gift of the copolymer to make SNPs. We thank Dr. Jimmy Mays for synthesis of the co-polymer to make CNPs. We thank Dr. John R. Dunlap for electron microscopy. We thank Tina Richey and Dr. Jonathan Wall for BALB/c mice. We thank Dr. David Kakhniashvili (UTHSC-Memphis) for mass spectrometry. We thank Sally Fridge for maintaining the mouse colonies.

#### Appendix A. Supplementary data

Supplementary data to this article can be found online at https://doi.org/10.1016/j.jconrel.2023.12.019.

#### References

- [1] M. Raith, S.J. Kauffman, M. Asoudeh, J.A. Buczek, N.-G. Kang, J.W. Mays, P. Dalhaimer, Elongated PEG-based nanoparticles bind the high-density lipoprotein (HDL) receptor scavenger receptor class B I (SR-BI), J. Control. Release 337 (2021) 448–457, https://doi.org/10.1016/j.jconrel.2021.07.045.
- [2] Y. Ju, J.M. Carreno, V. Simon, K. Dawson, F. Krammer, S.J. Kent, Impact of anti-PEG antibodies induced by SARS-CoV-2 mRNA vaccines, Nat. Rev. Immunol. 23 (2023) 135–136, https://doi.org/10.1038/s41577-022-00825-x.
- [3] G. Griffiths, J. Gruenberg, M. Marsh, J. Wohlmann, A.T. Jones, R.G. Parton, Nanoparticle entry into cells; the cell biology weak link, Adv. Drug Deliv. Rev. 188 (2022) 114403, https://doi.org/10.1016/j.addr.2022.114403.
- [4] M. Krieger, Scavenger receptor class B type I is a multiligand HDL receptor that influences diverse physiological systems, J. Clin. Investig. 108 (2001) 793–797.
- [5] M. Hadjidemetriou, Z. Al-Ahmady, K. Kostarelos, Time-evolution of in vivo protein corona onto blood-circulating PEGylated liposomal doxorubicin (DOXIL) nanoparticles, Nanoscale 8 (2016) 6948–6957, https://doi.org/10.1039/ c5nr09158f.
- [6] K. Kristensen, T.B. Engel, A. Stensballe, J.B. Simonsen, T.L. Andresen, The hard protein corona of stealth liposomes is sparse, J. Control. Release 307 (2019) 1–15, https://doi.org/10.1016/j.jcontrel.2019.05.042.
- [7] J.D. Gillmore, et al., CRISPR-Cas9 in vivo gene editing for transthyretin amyloidosis, N. Engl. J. Med. 385 (2021) 493–502, https://doi.org/10.1056/ NEJMoa2107454.

- [8] W. Ngo, et al., Identifying cell receptors for the nanoparticle protein corona using genome screens, Nat. Chem. Biol. 18 (2022) 1023–1031, https://doi.org/10.1038/ s41589-022-0109305.
- [9] P. Dalhaimer, B. Florey, S. Issac, Interactions of apolipoproteins with lipid-based nanoparticles. A.C.S, Nano 17 (2023) 837–842, https://doi.org/10.1021/ acsnano.2c10790.
- [10] A. Akinc, et al., Targeted delivery of RNAi therapeutics with endogenous and exogenous ligand-based mechanisms, Molecular Therapeutics 18 (2010) 1357–1364, https://doi.org/10.1038/mt.2010.85.
- [11] S.-D. Li, L. Huang, Stealth nanoparticles: high density but sheddable PEG is a key for tumor targeting, J. Control. Release 145 (2011) 178–181, https://doi.org/ 10.1016/j.iconrel.2010.03.016.
- [12] Y. Wang, et al., Age-associated disparity in phagocytic clearance affects the efficacy of cancer nanotherapeutics, Nat. Nanotechnol. (2023), https://doi.org/10.1038/ s41565-023-01502-3.
- [13] D. Neculai, et al., Structure of LIMP-2 provides functional insights with implications for SR-BI and CD36, Nature 504 (2013) 172–176, https://doi.org/ 10.1038/nature12684.
- [14] P. Dalhaimer, K.R. Blankenship, All-atom molecular dynamics simulations of polyethylene glycol (PEG) and LIMP-2 reveal that PEG penetrates deep into the proposed CD36 cholesterol-transport tunnel. A.C.S, Omega 7 (2022) 15728–15738, https://doi.org/10.1021/acsomega.2c00667.
- [15] M.A. Hillmyer, F.S. Bates, Synthesis and characterization of model polyalkane-poly (ethylene oxide) block copolymers, Macromolecules 29 (1996) 6994–7002, https://doi.org/10.1021/ma960774t.
- [16] K. Liu, et al., Multiomics analysis of naturally efficacious lipid nanoparticle coronas reveals high-density lipoprotein is necessary for their function, Nat. Commun. 14 (2023) 4007, https://doi.org/10.1038/s41467-023-39768-9.
- [17] Raith, et al., Obesity and inflammation influence pharmacokinetic profiles of PEG-based nanoparticles, J. Control. Release 355 (2023) 434–445, https://doi.org/10.1016/j.jconrel.2023.02.007.
- [18] P. Dalhaimer, F.S. Bates, D.E. Discher, Single molecule visualization of stiffness-tunable, flow-conforming worm micelles, Macromolecules 36 (2003) 6873–6877, https://doi.org/10.1021/ma034120d.
- [19] Y. Geng, P. Dalhaimer, S. Cai, R. Tsai, M. Tewari, T. Minko, D.E. Discher, Shape effects of filaments versus spherical particles in flow and drug delivery, Nat. Nanotechnol. 2 (2007) 249–255, https://doi.org/10.1038/nnano.2007.70.
- [20] N. Bertrand, et al., Mechanistic understanding of in vivo protein corona formation on polymeric nanoparticles and impact on pharmacokinetics, Nat. Commun. 8 (2017) 777, https://doi.org/10.1038/s41467-017-00600-w.
- [21] M. Ibrahim, et al., Investigation of anti-PEG antibody response to PEG-containing cosmetic products in mice, J. Control. Release 354 (2023) 260–267, https://doi. org/10.1016/j.jconrel.2023.01.012.
- [22] J. Santelices, M. Ou, W.W. Hui, G.H.B. Maegawa, M.J. Edelmann, Fluorescent labeling of small extracellular vesicles (EVs) isolated from conditioned media, Bio-Protoc. 12 (2022) e4447. https://doi.org/10.21769/BioProtoc.4447.
- [23] A. Hogenkamp, et al., Dietary fatty acids affect the immune system in male mice sensitized to ovalbumin or vaccinated with influenza, J. Nutr. 2011 (141) (2011) 698–702, https://doi.org/10.3945/jn.110.135863.
- [24] L.B. Ivashkiv, IFNy: signaling, epigenetics and roles in immunity, metabolism, disease and cancer immunotherapy, Nat. Rev. Immunol. 18 (2018) 545–558.
- [25] G. Toda, T. Yamauchi, T. Kadowaki, K. Ueki, Preparation and culture of bone-marrow-derived macrophages from mice for functional analysis, STAR Protocols 2 (2020) 100246, https://doi.org/10.1016/j.xpro.2020.100246.
- [26] I. Nakagawa, et al., Autophagy defends cells against invading group a streptococcus, Science 303 (2004) 1037–1040, https://doi.org/10.1126, science.1103966.
- [27] F. Meng, C.A. Lowell, Lipopolysaccharide (LPS)-induced macrophage activation and signal transduction in the absence of Src-family kinases hck, fgr, and lyn, J. Exp. Med. 185 (1997) 1661–1670, https://doi.org/10.1084/jem.185.9.1661.

- [28] L.D. Shultz, et al., Human lymphoid and myeloid cell development in NOD/LtSzscid II.2R gamma null mice engrafted with mobilized human hemopoietic stem cells, J. Immunol. 174 (2005) 6477–6489, https://doi.org/10.4049/ jimmunol.174.10.6477.
- [29] G. Miao, et al., Accelerated blood clearance of PEGylated nanoparticles induced by PEG-based pharmaceutical excipients, J. Control. Release 363 (2023) 12–26.
- [30] M. Asoudeh, N. Nguyen, et al., NCBI Gene Expression Omnibus (2023). GSE249596.
- [31] A. Kopp, M. Hebecker, E. Svobodova, M. Jozsi, Factor H: a complement regulator in health and disease, and a mediator of cellular interactions, Biomolecules 2 (2012) 46–75.
- [32] J. Losse, P.F. Zipfel, M. Jozsi, Factor H and factor H-related protein 1 bind to human neutrophils via complement receptor 3, mediate attachment to Candida albicans, and enhance neutrophil antimicrobial activity, J. Immunol. 184 (2010) 912–921.
- [33] M. Palmieri, et al., Characterization of the CLEAR network reveals an integrated control of cellular clearance pathways, Hum. Mol. Genet. 20 (2011) 3852–3866, https://doi.org/10.1093/hmg/ddr306.
- [34] A.G. Jay, A.N. Chen, M.A. Paz, J.P. Hung, J.A. Hamilton, CD36 binds oxidized low density lipoprotein (LDL) in a mechanism dependent upon fatty acid binding, J. Biol. Chem. 290 (2015) 4590–4603.
- [35] C.R. Stewart, et al., CD36 ligands promote sterile inflammation through assembly of a toll-like receptor 4 and 6 heterodimer, Nat. Immunol. 11 (2009) 155–161.
- [36] A. Etzerodt, S.K. Moestrup, CD163 and inflammation: biological, diagnostic, and therapeutic aspects, Antioxid. Redox Signal. 2013 (18) (2013) 2352–2363.
- [37] A. Al-Jarallah, B. Trigatti, A role for the scavenger receptor, class B type I in high density lipoprotein dependent activation of cellular signaling pathways, Biochim. Biophys. Acta 1801 (2010) 1239–1248, https://doi.org/10.1016/j. bbalip.2010.08.006.
- [38] R.P. McGlinchey, J.C. Lee, Cysteine cathepsins are essential in lysosomal degradation of α-synuclein, Proceedings of the National Academy of Sciences – U.S. A. 112 (2015) 9322–9327.
- [39] U.C. Anozie, P. Dalhaimer, Molecular links among non-biodegradable nanoparticles, reactive oxygen species, and autophagy, Adv. Drug Deliv. Rev. 122 (2017) 65–73, https://doi.org/10.1016/j.addr.2017.01.001.
- [40] V. Marx, Autophagy: eat thyself, sustain thyself, Nat. Methods 12 (2015) 1121–1125, https://doi.org/10.1038/nmeth.3661.
- [41] D.M. Sabatini, H. Erdjument-Bromage, M. Lui, P. Tempst, S.H. Snyder, RAFT1: a mammalian protein that binds to FKBP12 in a rapamycin-dependent fashion is homologous to yeast TORs, Cell 78 (1994) 35–43, https://doi.org/10.1016/0092-8674(94)90570-3.
- [42] R. Gerster, J.J. Eloranta, M. Hausmann, P.A. Ruiz, J. Cosin-Roger, A. Terhalle, U. Ziegler, G.A. Kullak-Ublick, A. von Eckardstein, G. Rogler, Anti-inflammatory function of high-density lipoproteins via autophagy of lkB kinase, Cell. Mol. Gastroenterol. Hepatol. 1 (2015) 171–187, https://doi.org/10.1016/j. jcmgh.2014.12.006.
- [43] L. Cai, Z. Wang, J.M. Meyer, A. Ji, D. van der Westhuyzen, Macrophage SR-BI regulates LPS-induced pro-inflammatory signaling in mice and isolated macrophages, J. Lipid Res. 53 (2012) 1472–1481, https://doi.org/10.1194/jlr. M023234.
- [44] G.T. Kozma, T. Shimizu, T. Ishida, J. Szebeni, Anti-PEG antibodies: properties, formation, testing and role in adverse immune reactions to PEGylated nanobiopharmaceuticals, Adv. Drug Deliv. Rev. 154 (2020) 163–175, https://doi.org/10.1016/j.addr.2020.07.024.
- [45] H. Zhou, et al., Dense and dynamic polyethylene glycol shells cloak nanoparticles from uptake by liver endothelial cells for long blood circulation, A.C.S. Nano 12 (2018) 10130–10141.